THE JOURNAL OF COMPARATIVE NEUROLOGY 460:597–611 (2003)

Rabbit Forebrain Cholinergic System: Morphological Characterization of Nuclei and Distribution of Cholinergic Terminals in the Cerebral Cortex and Hippocampus

CSABA VARGA,[I] WOLFGANG HÄRTIG,[I] JENS GROSCHE,[I] JAN KEIJSER,[f] PAUL G.M. LUITEN,[f] JOHANNES SEEGER,[j] KURT BRAUER,[ê] AND TIBOR HARKANY[f]*

[I]Department of Neurochemistry, Paul Flechsig Institute for Brain Research, University of Leipzig, D-04109 Leipzig, Germany
[I]Department of Neurophysiology, Paul Flechsig Institute for Brain Research, University of Leipzig, D-04109 Leipzig, Germany
[f]Department of Molecular Neurobiology, University of Groningen, NL-9750 AA Haren, The Netherlands
[j]Department of Anatomy, Histology and Embryology, University of Leipzig, D-04103 Leipzig, Germany
[ê]Department of Neuroanatomy, Paul Flechsig Institute for Brain Research, University of Leipzig, D-04109 Leipzig, Germany
[ê]Laboratory for Molecular Neurobiology, Department of Medical Biochemistry and Biophysics, Karolinska Institutet, S-17177 Stockholm, Sweden

ABSTRACT

Although the rabbit brain, in particular the basal forebrain cholinergic system, has become a common model for neuropathological changes associated with Alzheimer's disease, detailed neuroanatomical studies on the morphological organization of basal forebrain cholinergic nuclei and on their output pathways are still awaited. Therefore, we performed quantitative choline acetyltransferase (ChAT) immunocytochemistry to localize major cholinergic nuclei and to determine the number of respective cholinergic neurons in the rabbit forebrain. The density of ChAT-immunoreactive terminals in layer V of distinct neocortical territories and in hippocampal subfields was also measured. Another cholinergic marker, the low-affinity neurotrophin receptor ($p75^{NTR}$), was also employed to identify subsets of cholinergic neurons. Double-immunofluorescence labeling of ChAT and $p75^{NTR}$, calbindin D-28k (CB), parvalbumin, calretinin, neuronal nitric oxide synthase (nNOS), tyrosine hydroxylase, or substance P was used to elucidate the neuroanatomical borders of cholinergic nuclei and to analyze the neurochemical complexity of cholinergic cell populations. Cholinergic projection neurons with heterogeneous densities were found in the medial septum, vertical and horizontal diagonal bands of Broca, ventral pallidum, and magnocellular nucleus basalis (MBN)/substantia innominata (SI) complex; cholinergic interneurons were observed in the caudate nucleus, putamen, accumbens nucleus, and olfactory tubercule, whereas the globus pallidus was devoid of cholinergic nerve cells. Cholinergic interneurons were frequently

Grant sponsor: Deutsche Forschungsgemeinschaft; Grant number: Ha 2211/2-1 (W.H.); Grant sponsor: Interdisciplinary Center for Clinical Research at the University of Leipzig; Grant number: IZKF 01KS 9504 (J.G.); Grant sponsor: European Commission; Grant number: QLK-6-CT-1999-02112 (K.B.); Grant sponsor: Hungarian National Science Foundation (OTKA); Grant number: F035254 (T.H.).

*Correspondence to: Tibor Harkany, Laboratory for Molecular Neurobiology, Department of Medical Biochemistry and Biophysics, Scheeles väg 1:A1, Karolinska Institutet, S-17177 Stockholm, Sweden.
E-mail: tibor.harkany@mbb.ki.se

Received 8 May 2002; Revised 13 December 2002; Accepted 3 February 2003

DOI 10.1002/cne.10673

Published online the week of April 21, 2003 in Wiley InterScience (www.interscience.wiley.com).

present in the hippocampus and to a lesser extent in cerebral cortex. Cholinergic projection neurons, except those localized in SI, abundantly expressed $p75^{NTR}$, and a subset of cholinergic neurons in posterior MBN was immunoreactive for CB and nNOS. A strict laminar distribution pattern of cholinergic terminals was recorded both in the cerebral cortex and in CA1–CA3 and dentate gyrus of the hippocampus. In summary, the structural organization and chemoarchitecture of rabbit basal forebrain may be considered as a transition between that of rodents and that of primates. J. Comp. Neurol. 460:597–611, 2003.

Indexing terms: calcium-binding protein; choline acetyltransferase; confocal laser scanning microscopy; p75 low-affinity neurotrophin receptor; mapping

The basal forebrain (BFB) cholinergic system is involved in the regulation of a broad range of brain functions (Dunnett et al., 1991; Rasmusson, 2000; Semba, 2000). In particular, tonic cholinergic input to the cerebral cortex and hippocampus contributes to learning processes and memory consolidation and retrieval (Everitt and Robbins, 1997; Sarter and Bruno, 1999, Rasmusson, 2000). In addition, cholinergic neurons of the BFB also participate in the control of attention (Everitt and Robbins, 1997) as well as in the sleep/wake cycle (Semba, 2000). Multiple levels of evidence from both human and animal studies indicate that damage to cholinergic projection systems correlates with the development of cognitive impairment (Schliebs, 1998; Iraizoz et al., 1999; Harkany et al., 2000; Berger-Sweeney et al., 2001). Therefore, a causal relationship between cholinergic dysfunction and the progression of memory deficit in neurodegenerative disorders, such as Alzheimer's disease (AD), has been postulated.

In mammalian species investigated so far, the BFB cholinergic system consists of several interrelated nuclei that correspond with the Ch1–Ch4 regions as designated by Mesulam et al. (1983a, b). In general terms, cholinergic magnocellular projection neurons of the medial septum (MS) and vertical diagonal band of Broca (VDB) form the Ch1 and Ch2 subdivisions, respectively; the horizontal diagonal band of Broca (HDB) corresponds well with the Ch3 region, and cholinergic neurons situated in the ventral pallidum (VP), medullary laminae of the globus pallidus (GP), and magnocellular nucleus basalis (also termed *nucleus basalis of Meynert* for human)/substantia innominata complex (MBN/SI) have been regarded as major constituents of the Ch4 subdivision. Cholinergic projection neurons provide topologically strictly defined projections to remote areas, such as the cerebral cortex, hippocampus, thalamic nuclei, olfactory bulb, and amygdala (Armstrong et al., 1983; Mesulam et al., 1983b; Saper, 1984; Kása, 1986; Eckenstein et al., 1988; Brückner et al., 1992; Semba, 2000). Tract-tracing studies demonstrated that the MS and VDB are major sources of cholinergic terminals in the hippocampus; anterior, intermediate, and posterior subregions of the MBN innervate distinct areas of the cortical mantle, whereas cholinergic neurons of the VP and SI project to the amygdala (Mesulam et al., 1983b; Baisden et al., 1984; Rye et al., 1984; Ingham et al., 1985; Luiten et al., 1987). In their target regions, cholinergic fibers terminate on both excitatory (e.g., glutamatergic) and inhibitory (e.g., γ-aminobutyric acidergic) neurons, where acetylcholine-mediated modulation of the firing activity of target cells provides the anatomical substrate for the cholinergic control of a wide range of brain functions (Freund and Antal, 1988; Rasmusson, 2000). In addition to cholinergic projection neurons, cholinergic interneurons have frequently been found in striatal regions, the cerebral cortex (Sofroniew et al., 1982; Houser et al., 1985), and the hippocampus of different mammalian species (Freund and Buzsáki, 1996; Frotscher et al., 2000).

Structural organization of cholinergic BFB nuclei and the topography of their projections have been the subjects of investigations in several mammalian species, including rat (Bigl et al., 1982; Armstrong et al., 1983; Mesulam et al., 1983a), cat (Kimura et al., 1981), rhesus monkey (Mesulam et al., 1983a; Geula et al., 1993), and human (Geula et al., 1993). Although major neuroanatomical characteristics of cholinergic BFB nuclei are apparently similar in the mammalian species studied, important species-specific differences were also identified (Geula et al., 1993). These include, for example, the relative reduction of MS and VDB; appearance of septum pellucidum; topological organization of the VP and the MBN/SI complex; and localization of the capsulae interna, externa, and extrema. From a neurochemical point of view, 1) selective expression of the low-affinity neurotrophin receptor p75 ($p75^{NTR}$) in cholinergic neurons of all mammalian species (Mufson et al., 1989; Maclean et al., 1997; Tremere et al.,

Abbreviations

AcSh	shell of nucleus accumbens
AD	Alzheimer's disease
BFB	basal forebrain
CB	calbindin D-28k
ChAT	choline-acetyltransferase
CR	calretinin
Cy	carbocyanine
GP	globus pallidus
HDB	horizontal diagonal band of Broca
ir	immunoreactive
MBN	magnocellular nucleus basalis/nucleus basalis of Meynert
MS	medial septum
NCa	caudate nucleus
nNOS	neuronal nitric oxide synthase
$p75^{NTR}$	low-affinity neurotrophin receptor p75
PB	phosphate buffer
PV	parvalbumin
Pu	putamen
SI	substantia innominata
SP	substance P
TBS	Tris-buffered saline
TBS-BSA	Tris-buffered saline containing 2% bovine serum albumin
TH	tyrosine-hydroxylase
VDB	vertical diagonal band of Broca
VP	ventral pallidum

2000); 2) the presence of calbindin D-28k (CB) in cholinergic neurons of primates, including humans (Chang and Kuo, 1991; Côté and Parent, 1992; Geula et al., 1993; Ichitani et al., 1993; Härtig et al., 2002); and 3) coexpression of neuronal (constitutive) nitric oxide synthase (nNOS) in subsets of rat BFB cholinergic neurons (Schober et al., 1989; Brauer et al., 1991; Geula et al., 1993) illustrate profound phylogenetic differences that may substantially influence the sensitivity of cholinergic neurons of different mammalian species to aging and to experimental manipulations.

Recent experimental data indicate that the rabbit brain might be in several respects appropriate for modeling multiple neurochemical characteristics of AD, inasmuch as subcortical denervation by means of ME20.4-saporin induced selective cholinergic immunolesions (Beach et al., 2000), and feeding with diets containing high cholesterol concentrations was shown to trigger the formation of senile plaque-like β-amyloid deposits in the rabbit cerebral cortex (Sparks et al., 1994, 1995, 2000). In spite of the growing interest in using the rabbit for modeling cholinergic dysfunction, detailed neuroanatomical studies on the organization of cholinergic components of the rabbit BFB are still lacking. In fact, only a few neuroanatomical descriptions based on classical histological techniques (Winkler and Potter, 1911; Monnier and Gangloff, 1961; Urban and Richard, 1972) and immunohistochemical studies (McGeer et al., 1974; Kan et al., 1978; Chao et al., 1982; Baisden et al., 1984) have addressed the localization of cholinergic nuclei in rabbit brain. These studies fell short, however, because of either the only superficial localization of cholinergic nuclei or partly insufficient choline acetyltransferase (ChAT; EC 3.2.1.6) immunolabeling (as described in detail by Rossier, 1981). In the present study, therefore, we performed sensitive immunoperoxidase labeling of ChAT and $p75^{NTR}$ on serial sections spanning all major cholinergic BFB nuclei as well as cerebral cortical and dorsal hippocampal projection areas to map their structural organization and to measure the number and density of cholinergic nerve cells and of their cortical and hippocampal projections. Moreover, additional series of sections were double-labeled for ChAT and $p75^{NTR}$, the calcium-binding proteins parvalbumin (PV), calretinin (CR), CB, nNOS, tyrosine hydroxylase (TH), or substance P (SP) to identify the neurochemical heterogeneity and spatial relationships of cholinergic BFB neuron populations. Although our primary aim was to investigate the Ch1–Ch4 areas, we also studied the striatal regions, where large cholinergic interneurons exhibit some differences in their $p75^{NTR}$ expression in some animal species investigated to date (Kokaia et al., 1998; Ferreira et al., 2001).

MATERIALS AND METHODS

Animals, perfusion, and sectioning

New Zealand white rabbits of both sexes (n = 7, 2.3–5.1 kg, 4–15 months of age) were used in this study. The animals were deeply anesthetized with a mixture of ketamine (50 mg/kg body weight; Exalgon; Merck, Hallbergmoos, Germany) and xylazine (4 mg/kg body weight; Rompun; Bayer AG, Leverkusen, Germany). Subsequently, the rabbits were transcardially perfused with 800 ml of 4% paraformaldehyde containing 0.1% glutaraldehyde in phosphate-buffer (PB; 0.1 M, pH 7.4) that was preceded by a prerinse with ice-cold physiological saline (150 ml). Whole brains were removed from the skull, divided into fore- and hindbrain regions, and postfixed in 4% paraformaldehyde overnight. All efforts were made to minimize the number of animals and their suffering throughout the perfusion procedure. Their care and treatment were in accordance with European Communities Council Directive 86/609/EEC and were approved by the Local Ethical Committee of the University of Leipzig (TVV-Nr. 15/00).

For cryoprotection, forebrain samples were equilibrated in 30% sucrose in PB for at least 48 hours. Thirty-micrometer thick coronal sections were cut on a freezing microtome and collected individually in Tris-buffered saline (TBS; 0.1 M, pH 7.4). Sectioning started at the anterior pole of the MS and spanned the entire BFB, including the caudal pole of the MBN/SI complex, yielding about 250 sections in each individual case. To ensure standard cross-sectional distances throughout the quantification procedures, each sixth section was immunolabeled for ChAT; all consecutive sections were processed for $p75^{NTR}$ (both with nickel-enhanced 3,3′-diaminobenzidine as chromogen), whereas the successive series was used for Nissl staining. A fourth series of sections was applied to the immunofluorescence double labeling of ChAT and $p75^{NTR}$ and was pretreated with Sudan black B according to Schnell et al. (1999) to quench autofluorescence of the tissue and to reveal the myelination of fibers. To assess quantitatively the possible colocalization of CB and nNOS in cholinergic neurons, the fifth and sixth series of sections in two male and one female rabbits were used for double-immunofluorescence detection of CB/ChAT and nNOS/ChAT, respectively. For the carbocyanine (Cy) double-fluorescence staining of ChAT and a panel of additional neuronal markers (see Table 1), sections from the fifth series of one male rabbit and selected sections from two female animals were used without Sudan black B pretreatment. According to this sampling protocol, the cross-sectional distance amounted to 180 μm.

Immunohistochemical procedures

All immunohistochemical methods were performed on free-floating sections. Before immunoperoxidase staining, endogenous tissue peroxidase activity was abolished by treatment with 0.6% H_2O_2 in TBS for 30 minutes. For the immunoperoxidase labeling of ChAT, sections were then preincubated in 5% normal donkey serum (Jackson Immunoresearch, West Grove, PA) in TBS containing 0.3% Triton X-100 for 1 hour. Subsequently, tissue samples were incubated in affinity-purified goat anti-ChAT (Li and Furness, 1998; Reiche and Schemann, 1999; Chemicon International, Hofheim, Germany; 1:100 in TBS containing 0.3% Triton X-100 and 5% normal donkey serum) for 16 hours at room temperature. Subsequently, sections were thoroughly rinsed and exposed to biotinylated donkey anti-sheep IgG [highly cross-reacting with goat IgG (Jackson Immunoresearch); 1:500 in TBS containing 2% bovine serum albumin (TBS-BSA)] for 1 hour. Finally, sections were processed with preformed complexes of streptavidin and biotinylated peroxidase and stained with nickel-enhanced 3,3′-diaminobenzidine as chromogen (Härtig et al., 1995).

For the immunodetection of $p75^{NTR}$, nonspecific binding sites were blocked in 5% normal goat serum (Jackson

TABLE 1. List of Markers Used for Double-Immunofluorescence Labeling[1]

Marker	Host	Dilution	Source	Fluorochromated secondary antibody	Reference
Choline acetyltransferase	Goat	1:25 1:50	Chemicon, Hofheim, Germany	Cy2 donkey anti-goat Cy3 donkey anti-goat	Li and Furness, 1998 Reiche and Schemann, 1999
p75 Neurotrophin receptor	Mouse (clone ME 20.4)	1:2	Dr. A. Fine, Halifax, NS, Canada	Cy3 donkey anti-mouse	Ross et al., 1984
Calbindin D-28k	Mouse (clone CL-300)	1:200	Sigma, Deisenhofen, Germany	Cy2 donkey anti-mouse	Celio et al., 1990
Calretinin	Rabbit	1:300	SWant, Bellinzona, Switzerland	Cy2 donkey anti-rabbit	Schwaller et al., 1993
Parvalbumin	Mouse (clone PA-235)	1:300	SWant, Bellinzona, Switzerland	Cy2 donkey anti-mouse	Celio et al., 1988
Nitric oxide synthase, neuronal	Rabbit	1:200	Laboserv, Giessen, Germany	Cy2 donkey anti-rabbit	Alm et al., 1993
Substance P	Rabbit	1:1,000	DiaSorin, Stillwater, MN	Cy3 donkey anti-rabbit	Gall, 1988
Tyrosine hydroxylase	Rabbit	1:250	Chemicon, Hofheim, Germany	Cy3 donkey anti-rabbit	Haycock, 1987

[1]Panel of antibodies used to determine the neurochemical heterogeneity of cholinergic neurons in rabbit basal forebrain. Staining methods are described in detail in Materials and Methods. Cy, carbocyanine.

Immunoresearch) in TBS containing 0.3% Triton X-100 for 1 hour, followed by incubation of the sections in monoclonal mouse anti-p75^{NTR} antibody [clone ME 20.4, 1:5 (Ross et al., 1984); donated by Dr. A. Fine] in the blocking solution overnight. After extensive rinsing, sections were reacted with biotinylated goat anti-mouse IgG (Jackson Immunoresearch; 2.5 μg/ml in TBS-BSA) for 1 hour. Thereafter, tissue samples were processed according to a visualization protocol identical to that described for the immunodetection of ChAT (Härtig et al., 1995).

For the immunofluorescence double labeling of ChAT and other markers, sections were preincubated in TBS containing 0.3% Triton X-100 and 5% normal donkey serum for 1 hour. Sections were then exposed to a mixture containing both goat anti-ChAT and one of the primary mouse or rabbit antibodies listed in Table 1 in TBS containing 0.3% Triton X-100 and 5% normal donkey serum for 16 hours. The goat anti-ChAT antibody was applied in a 1:25 dilution and subsequently visualized by Cy2-conjugated donkey anti-goat IgG combined with the immunolabeling of p75^{NTR}, SP, and TH with Cy3-tagged secondary antibodies. In contrast, goat anti-ChAT antibody was used at a dilution of 1:50 and localized with Cy3-tagged donkey anti-goat IgG when CB, CR, PV, and nNOS were simultaneously revealed with Cy2 immunostaining (Table 1). All secondary antibodies were applied at a concentration of 20 μg/ml TBS-BSA for 1 hour and were obtained at the highest available purity (Jackson Immunoresearch).

Omission of the primary antibodies in control experiments caused the absence of any cellular staining. Moreover, switching of the fluorophores for the detection of ChAT and any other relevant markers resulted in labeling patterns identical to those yielded in the serial staining experiments. After the histochemical procedures, sections were extensively washed in TBS, dipped in distilled water, mounted on fluorescence-free slides, air dried, and coverslipped. The sections were covered either with Entellan in toluene (Merck, Darmstadt, Germany) or, when pretreated with Sudan black B, with glycerol/gelatin (Sigma, Deisenhofen, Germany).

Low-magnification mapping of BFB nuclei

Mapping of cholinergic BFB nuclei was carried out on ChAT (Fig. 1) and Nissl-stained sections at 2.5× primary magnification using a Leica LB100T microscope fitted with a high-resolution camera module (DC-100) that was attached to a Quantimet computerized image-analysis platform (Leica, Cambridge, United Kingdom). All sections were captured under identical illumination at 600 dpi resolution. Sections were systematically sampled to allow complete overview of the BFB, and composite images were assembled using Paint Shop Pro (v. 7.01; Jasc Software Inc., Eden Prairie, MN). Nissl-stained sections were used to delineate particular BFB nuclei (data not shown) and were then fitted with images obtained after ChAT immunocytochemistry to yield the schematic forebrain maps presented in Figure 1.

High-magnification microscopy

High-power photomicrographs of ChAT-ir neuron populations were prepared using a Zeiss Axioplan microscope equipped with an AxioCam high-resolution camera (Zeiss) at 1,030 × 1,300 pixel resolution. Captured images were uniformly processed for contrast and brightness adjustment using Paint Shop Pro (v. 7.01). Tissue samples double-labeled for ChAT and p75^{NTR}, CB, CR, PV, TH, nNOS, or SP were first inspected using a Zeiss Axioplan fluorescence microscope equipped with appropriate single- and double-bandpass filters (Nos. 15, 09, and 24). Images of selected specimens were then obtained using a Zeiss 510 confocal laser scanning microscope. After color coding, ChAT immunolabeling always appears in red, whereas structures immunoreactive for the simultaneously stained marker are shown in green. Panels of images were generated by CorelDraw (v. 10.0; Corel Corp., Ottawa, Ontario, Canada).

Quantitative image analysis

Morphometric analysis of major cholinergic nuclei, such as the MS, VDB, HDB, NCa, nucleus putamen (Pu), olfactory tubercule, accumbens nucleus, GP, VP, and MBN/SI complex was performed using a Leica Q-600HR computerized image-analysis system. Complete series of sections stained for ChAT with nickel-enhanced 3,3′-diaminobenzidine detection from three animals (two males and one female) were systematically sampled (35–40 sections/brain); brain regions of interest were manually delineated, and their surface area was determined (mm^2). Subsequently, the number of neuronal perikarya with clearly discernible nuclei was counted in each brain region, whereas clearly fragmented nerve cell profiles were excluded from the sampling protocol (Harkany et al., 2001a, b). Because cholinergic BFB neurons are distributed in a largely inhomogeneous manner, posing a potential bias in disector-based cell counts (West,

1993), disector analyses were not carried out. It is worth noting that recent studies in our laboratory revealed no considerable difference in the number of cholinergic MBN/SI neurons when analyzed by either disector or exhaustive counting protocols (Horvath et al., 2002). To correct for the possibility of overestimation of cell numbers, a Floderus correction factor was introduced as described by Palkovits et al. (1971). Briefly, the average size of cholinergic BFB nuclei was determined in all forebrain regions of interest, and a clearly discernible nucleus was considered as 8.9 μm in diameter (a; mean value). Insofar as intact neurons contained nuclei with an average radius of 5.7 μm (r), the Floderus correction factor was calculated as $f = 0.8077$ in 30-μm-thick sections (T_1), given that $f = T_1/[T_1 + \mathrm{sqrt}(r^2 - (a/2)2)]$. The probability of double cell counts, based on the 180-μm cross-sectional distance, was considered negligible. Thereafter, the average surface area of each brain region as well as the average number of ChAT-immunoreactive (ir) nerve cells was computed. Finally, by taking the length of each brain region along the z-axis, expressed as the number of sections spanned × 30 μm, into account, the volume of individual brain areas and the corresponding number of ChAT-ir neurons were estimated (Horvath et al., 2000, 2002). Neuron density was calculated as the ratio of the number of neurons and the volume of the particular brain region and expressed as cell number per cubic millimeter. An identical quantification protocol was applied when assessing the frequency of CB/ChAT and nNOS/ChAT colocalization, except that cell counts were performed using an appropriate double-bandpass filter (No. 24; Zeiss) for simultaneous detection of Cy2 and Cy3 signals.

The density of ChAT-ir projection fibers was determined in the cingulate cortex and in layer V of the retrosplenial cortex, forelimb, and hindlimb representations of the somatosensory cortex and in the parietal and occipital cortices (Fleischhauer at al., 1980; Zilles, 1985). Moreover, the density of ChAT-ir terminals in the dorsal hippocampus was also recorded, in which hippocampal subfields were defined according to Freund and Buzsáki (1996). Image analysis was performed using a standard protocol on a Quantimet Q-550IV image-analysis system (Harkany et al., 2000, 2001a, b) in all sections employed for quantification of cell numbers. Briefly, after background subtraction and gray-scale threshold determination, the surface area of skeletonized ChAT-ir fibers ([the area covered by ChAT-positive cholinergic fibers]/[the total sampling area], given as percentages) was computed in each section using a 470-nm emission filter. Data on the volume of cholinergic nuclei, total numbers and density of the nerve cells, percentage of colocalization for CB/ChAT and nNOS/ChAT, and area density of cortical cholinergic projections were expressed as mean ± SEM.

Nomenclature

Cholinergic nuclei were identified according to the brain maps of Winkler and Potter (1911) and Urban and Richard (1972). In cases in which the anatomical description of a particular brain structure was not available, it was identified based on the corresponding structure in rat brain (Paxinos and Watson, 1986). Our nomenclature conformed to that introduced by Mesulam et al. (1983a, b) for the rhesus monkey and rat, but with some modifications because of interspecies differences (Butcher and Semba, 1989). Importantly, ChAT immunocytochemistry alone during the quantification process did not allow unequivocal delineation of the anatomical boundaries of VP, MBN, and SI, the latter made up of $p75^{NTR}$-immunonegative cholinergic neurons, so we subdivided these territories as VP and the largely diffuse MBN/SI complex. Delineation of cortical areas adhered to mapping studies in the cerebral cortex of rabbit (Fleischhauer et al., 1980) and rat (Zilles, 1985).

RESULTS

General considerations

Rostrally, the MS appears as a small, compact nucleus in the midline of the brain and is surrounded by the lateral septal nuclei (Fig. 1A,A′,B,B′). After gradual expansion, the MS reaches its maximal extent approximately at the coronal plain of bregma (Urban and Richard, 1972; Fig. 1B,B′), whereas the fornix, as its major output pathway innervating the hippocampus, appears more caudally (Fig. 1C,C′,D,D′). Whereas the dorsal and lateral boundaries of the MS are clearly discernible, a more dispersed group of cholinergic neurons, termed the VDB, neighbors the MS ventrally (Fig. 1B,B′). Because of the close proximity of these nuclei, they can be designated as the MS/VDB complex. Similarly to the organization of the rat BFB, the HDB is located lateroventrally from the VDB. Along the longitudinal axis of rabbit brain, the HDB extends laterally (Fig. 1B,B′,C,C′). Subsequent to the disappearance of the compact group of cholinergic HDB neurons, the MBN forms the most caudal part of cholinergic BFB projection neurons in rabbit forebrain (Fig. 1D–F′). Tract-tracing studies in the rat BFB revealed that three, namely, the anterior, intermediate, and posterior, MBN subdivisions can be distinguished (Luiten et al., 1987; Gaykema et al., 1990). In the present study, we used the nomenclature of Gaykema et al. (1990) and identified the anterior MBN as extending caudally to the disappearance of the anterior commissure (Fig. 1D,D′), the intermediate MBN subdivision adjacent to the ventromedial surface of the GP (Fig. 1E,E′), and the compact posterior MBN subdivision (Fig. 1F,F′). A diffuse population of cholinergic neurons situated ventromedially from the intermediate MBN forms the SI. Because ChAT immunolabeling does not provide a clear demarcation between these nuclei, they were further assigned as the MBN/SI complex.

The capsula interna served for anatomical separation between the NCa and the Pu, which contained large cholinergic interneurons (Fig. 1A′–F′). Interestingly, a well-separated ventral subregion of the Pu, referred to as the ventral putamen (Fig. 1C,C′), could also be identified. In conjunction with the disappearance of the core and shell (AcSh) divisions of the nucleus accumbens, which are located ventromedially from the NCa and are often assigned as parts of the ventral striatum, the medial segment of the Pu borders the GP. The GP extends in the caudal direction and is enveloped by cholinergic neurons of the MBN (Fig. 1D,D′,E,E′).

BFB cholinergic neurons provide innervation to several grisea in the rabbit forebrain. Whereas the present study was focused on cortical and hippocampal cholinergic projections, dense ChAT-immunoreactive (-ir) innervation was also visualized in the olfactory tubercule (Fig. 1A,A′,B,B′), the anteroventral thalamic nucleus (Fig. 1F,F′), and the cortical, central, and basolateral amygdaloid nuclei (Fig. 1F,F′).

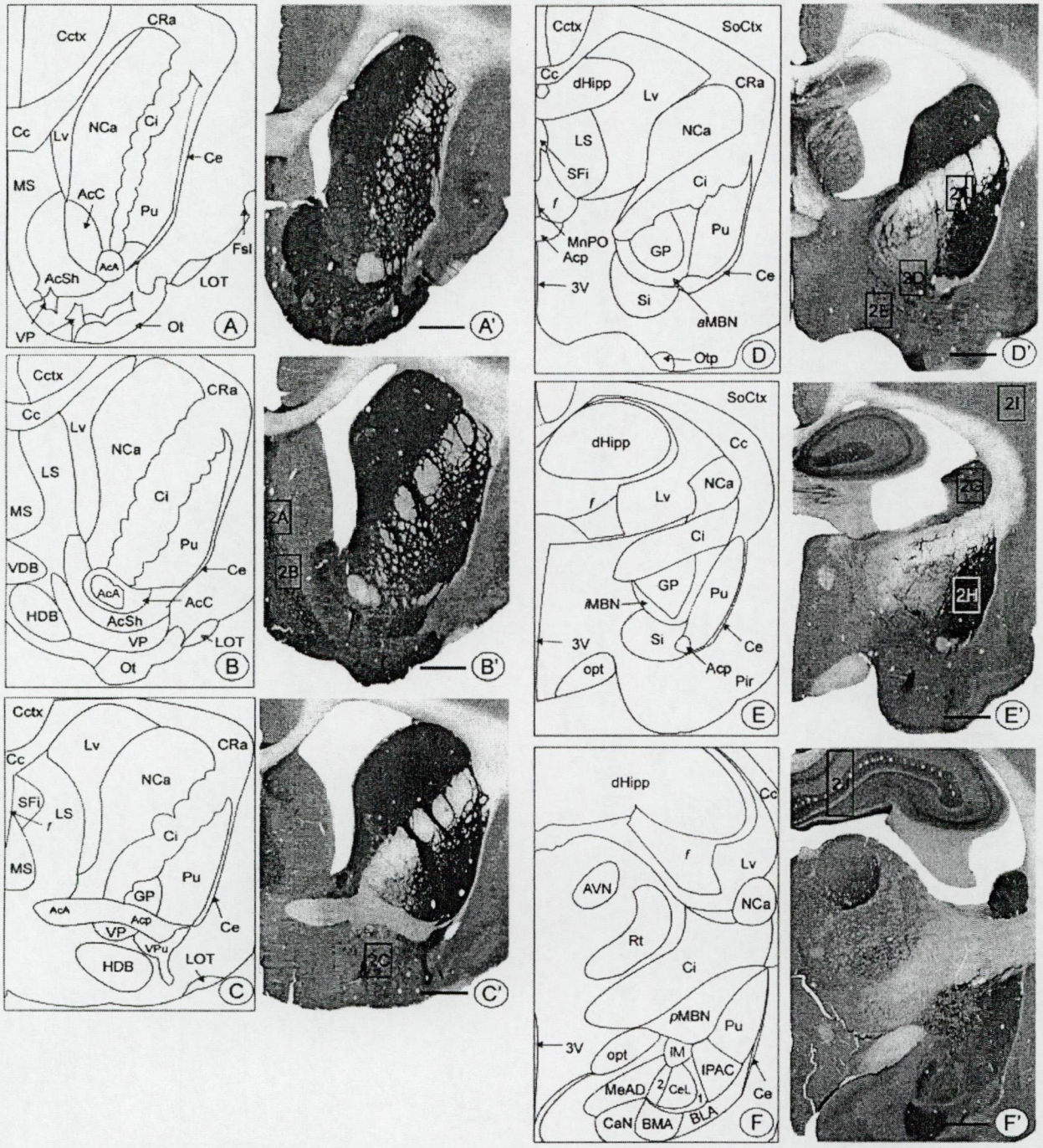

Fig. 1. Distribution of cholinergic basal forebrain (BFB) nuclei in rabbit forebrain. **A–F** represent schematic maps of major BFB nuclei that were prepared using sections stained for choline acetyltransferase (**A′–F′**). Details of the imaging procedure and particular anterior-posterior coordinates of the captured planes are referred to in the text. Nuclei were identified and termed according to the nomenclature introduced by Winkler and Potter (1911) and Urban and Richard (1972), in conjunction with particular designations of Paxinos and Watson (1986) in rat brain. Numbered territories (2A–2J) correspond to the high-power images shown in Figure 2. 1, Central amygdaloid nucleus, capsular subdivision; 2, central amygdaloid nucleus, medial subdivision; 3V, third ventricle; AcA, comissura anterior, anterior part; AcC, accumbens nucleus, core; Acp, commissura anterior, posterior part; AcSh, accumbens nucleus, shell; AVN, anteroventral thalamic nucleus; BLA, basolateral amygdaloid nucleus; BMA, basomedial amygdaloid nucleus; CA, central amygdaloid nucleus; CaN, cortical amygdaloid nucleus; Cc, corpus callosum; Cctx, cingulate cortex; Ce, capsula externa; CeL, central amygdaloid nucleus, lateral subdivision; Ci, capsula interna; CRa, capsula radiata; dHipp, dorsal hippocampus; f, fornix; Fsl, fissura sagittalis lateralis; GP, globus pallidus; HDB, horizontal diagonal band of Broca; IM, intercalated amygdaloid nucleus; IPAC, interstitial nucleus of posterior limb of accumbens; LOT, lateral olfactory tract; LS, lateral septum; Lv, lateral ventricle; (a,i,p)MBN, magnocellular basal nucleus (anterior, intermediate, and posterior subdivisions); MeAD, medial amygdaloid nucleus, anterodorsal division; MnPO, median preoptic nucleus; MS, medial septum; NCa, nucleus caudatus; opt, optic tract; Ot, olfactory tubercule; Otp, olfactory tubercule, posterior part; Pir, piriform cortex; Pu, putamen; Rt, reticular thalamic nucleus; SFi, septofimbrial nucleus; SI, substantia innominata; SoCtx, somatosensory cortex; VDB, vertical diagonal band of Broca; VP, ventral pallidum; VPu, putamen, ventral subdivision. Scale bars = 1.2 mm.

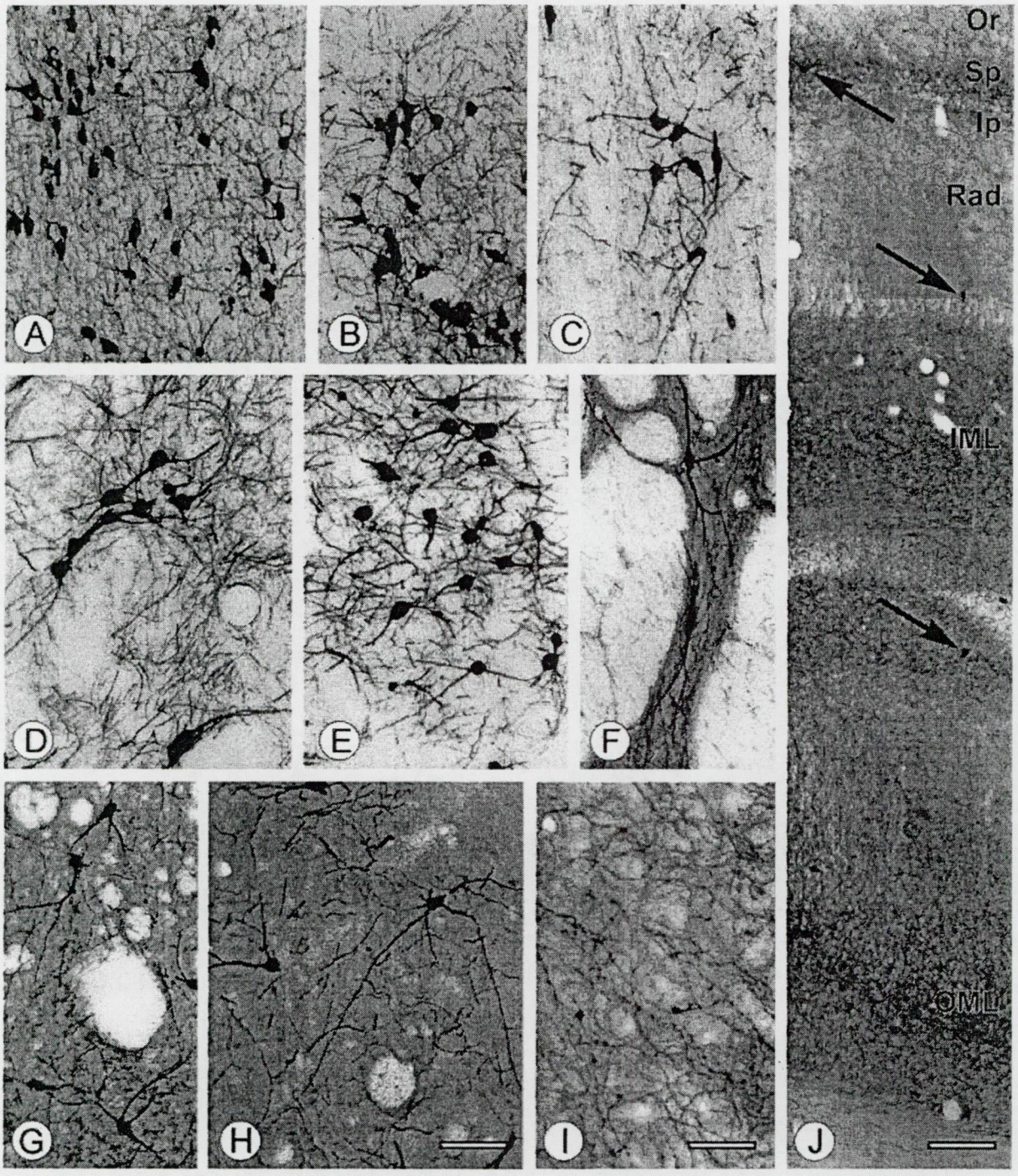

Fig. 2. Distribution of choline acetyltransferase (ChAT)-immunoreactive neurons in the rabbit basal forebrain (**A–H**) and of cholinergic terminals in the somatosensory cortex (hindlimb area; **I**) and dorsal hippocampus (**J**). Clusters of multipolar cholinergic nerve cells were demonstrated in the medial septum (A) and vertical (B) and horizontal (C; HDB) diagonal bands of Broca. Note that C depicts spindle-shaped ChAT-ir neurons in the posterior subdivision of the HDB. Cholinergic neurons in the magnocellular nucleus basalis (MBN; D) and substantia innominata (SI; E) formed a largely interrelated neuronal network in which MBN neurons appeared larger than SI neurons. It is worth noting that MBN neurons were intermingled with densely stained passing cholinergic fiber bundles (D). ChAT-ir neurons were frequently found in cell bridges between the nucleus caudatus (NCa) and putamen (Pu, F). Moreover, multipolar cholinergic interneurons of similar size and density were observed in NCa (G) as well as in Pu (H). A dense ChAT-ir fiber network was visualized throughout the cerebral cortex and exhibited a clear laminar distribution pattern. The highest density of cholinergic fibers was seen in layer V of the cerebral cortex (I). Cholinergic terminals in the hippocampus also showed strict topographical distribution. J is a reconstruction of the dorsal hippocampus, with the highest ChAT-ir terminal density in the stratum suprapyramidale (Sp) of the CA1 and CA3 subfields. Note the frequent presence of ChAT-ir interneurons (arrows). IML, inner molecular layer of the dentate gyrus; Ip, stratum infrapyramidale; OML, outer molecular layer of the dentate gyrus; Or, stratum oriens; Rad, stratum radiatum. Scale bar in H = 150 μm for A–H; bar in I = 50 μm; bar in J = 280 μm.

TABLE 2. Morphometric Parameters of Cholinergic Nuclei in Rabbit Basal Forebrain as Revealed by Choline Acetyltransferase (ChAT) Immunocytochemistry[1]

Brain region	Subdivision	Volume (mm^3)	Total cell number	Cell density
Nucleus caudatus	Anterior	13.9 ± 0.8	3,447 ± 367	177 ± 21
	Intermediate	8.1 ± 0.2	1,018 ± 78	89 ± 8
	Posterior	5.6 ± 0.9	659 ± 116	84 ± 6
Putamen	Anterior	7.1 ± 0.9	2,264 ± 290	227 ± 15
	Intermediate	5.5 ± 0.1	1,964 ± 134	250 ± 15
	Posterior	8.9 ± 1.3	2,387 ± 168	196 ± 14
Medial septum		4.7 ± 0.4	6,426 ± 1351	963 ± 218
Vertical diagonal band of Broca		1.3 ± 0.1	3,028 ± 209	1,717 ± 269
Horizontal diagonal band of Broca		1.8 ± 0.1	5,420 ± 727	2,087 ± 303
Shell of nucleus accumbens		4.9 ± 0.9	2,387 ± 267	373 ± 56
Ventral pallidum		1.8 ± 0.5	873 ± 225	331 ± 20
Nucleus basalis magnocellularis	Anterior	1.5 ± 0.1	2,006 ± 114	735 ± 98
and substantia innominata	Intermediate	2.14 ± 0.1	2,312 ± 249	994 ± 168
	Posterior	1.5 ± 0.3	2,806 ± 612	960 ± 81

[1]Details of the sampling scheme, image-analysis protocol, and delineation of subdivisions of nucleus caudatus (NCa), putamen (Pu), and magnocellular nucleus basalis (MBN)/substantia innominata (SI) complex are described in Materials and Methods. Because ChAT immunocytochemistry alone did not allow unequivocal separation of MBN from SI, these two nuclei were regarded as the MBN/SI complex. Total numbers of nerve cells refer to the amount of neurons in the entire volume of a particular brain region, and neuronal density is reported as number of nerve cells per cubic millimeter. Data represent means ± SEM.

Medial septum and vertical limb of the diagonal band of Broca

Dense clusters of cholinergic neurons of the MS/VDB complex become already visible with low magnification (Fig. 1A′,B′). Within the boundaries of the MS, ChAT-ir neurons are concentrated along the midline raphe of the septum and the outer edge of the nucleus and form mirror-symmetrical, shell-like cell assemblies. The highest density of cholinergic cells can be found within some 100 μm from midline (Figs. 1B′, 2A). This laminar organization was less apparent in the VDB (Fig. 2B). Whereas the absolute number of ChAT-ir cells in the MS is approximately twofold higher than that in the VDB, the above-mentioned nonhomogeneous distribution of ChAT-ir neurons in the MS results in a lower mean density of nerve cells (Table 2). Cholinergic projection neurons in the MS and VDB were of intermediate size and appeared as bipolar or multipolar nerve cells (Fig. 2A,B). Double-immunofluorescence labeling for ChAT and $p75^{NTR}$ revealed a virtually complete colocalization of the two cholinergic markers (Fig. 3A,A′,B,B′). None of the additional markers was coexpressed in cholinergic perikarya (see, e.g., Fig. 4C,D,H).

Horizontal limb of the diagonal band of Broca

In general terms, the cytoarchitecture of the HDB resembles that of the VDB, in which a dense cluster of multipolar ChAT-ir neurons is present (Fig. 1B′,C′). High-power microscopy in the posterior region of the HDB—corresponding to Figure 1C′—often revealed spindle-shaped ChAT-ir perikarya (Fig. 2C). Quantitative analysis of cholinergic cell numbers in the HDB demonstrated the highest density of ChAT-ir neurons among the cholinergic BFB nuclei investigated (Table 2). Similarly to the case in the MS and VDB, all ChAT-ir neurons exhibited $p75^{NTR}$ immunoreactivity (data not shown), whereas none of the other markers showed colocalization with cholinergic HDB neurons (see, e.g., Fig. 4H).

Pallidum

The rostral expansion of the VP is emerging already at the level of the first appearance of the MS (Fig. 1A,A′) and is often interrupted by striatal cell bridges between the olfactory tubercule and the AcSh. The neuropil is less densely stained for ChAT than the surrounding striatal regions (Fig. 1A′). In parallel with the disappearance of AcSh, the VP expands under the commissura anterior, whereas more caudally it seems to become identical with the SI. Cholinergic neurons situated in the VP region are similar in their morphological characteristics, density, and size to those of the AcSh (Table 2). Double-immunofluorescence labeling, however, revealed that ChAT-ir neurons in the VP, but not in the AcSh, express $p75^{NTR}$. The GP itself lacks any cellular ChAT labeling and, concomitantly with its caudal extension, becomes encircled by a ribbon-like cluster of cholinergic magnocellular neurons that make up the MBN (Fig. 1D′,E′).

Magnocellular nucleus basalis/substantia innominata complex

Concomitantly with the disappearance of the commissura anterior, the anterior MBN subdivision can be distinguished, followed by the major—intermediate—part that transits into the compact posterior MBN subdivision. MBN neurons form clusters consisting of 5–20 ChAT-ir cells that are surrounded by densely stained fiber bundles (Fig. 2D). These cholinergic cell clusters exhibit a heterogeneous distribution pattern; e.g., some MBN-related neurons are also visible in the internal lamina between the Pu and GP as well as in the capsula interna (Fig. 3C). Whereas subsets of ChAT-ir neurons of different sizes can be observed in this region, ChAT immunolabeling alone did not allow the unambiguous delineation of definite boundaries between the MBN and the SI, the latter being generally found ventromedially from the MBN in other mammalian species. Therefore, cell counts were performed on the entire MBN/SI complex, where present, and on the posterior subdivision of the MBN (Fig. 1F′) and revealed a gradual rostrocaudal increase in the total numbers of ChAT-ir neurons (Table 2).

A dorsal-to-ventral descending gradient of $p75^{NTR}$-ir neurons was present in the intermediate MBN/SI. Double-immunofluorescence labeling for ChAT and $p75^{NTR}$ confirmed the presence of neurochemically distinct subpopulations of cholinergic neurons (Fig. 3C,C′). Whereas virtually all large cholinergic nerve cells in the dorsolateral MBN/SI complex were immunoreactive for $p75^{NTR}$, a subpopulation of medium-sized cholinergic neurons (Fig. 2E) was immunonegative for $p75^{NTR}$ in the ventromedial

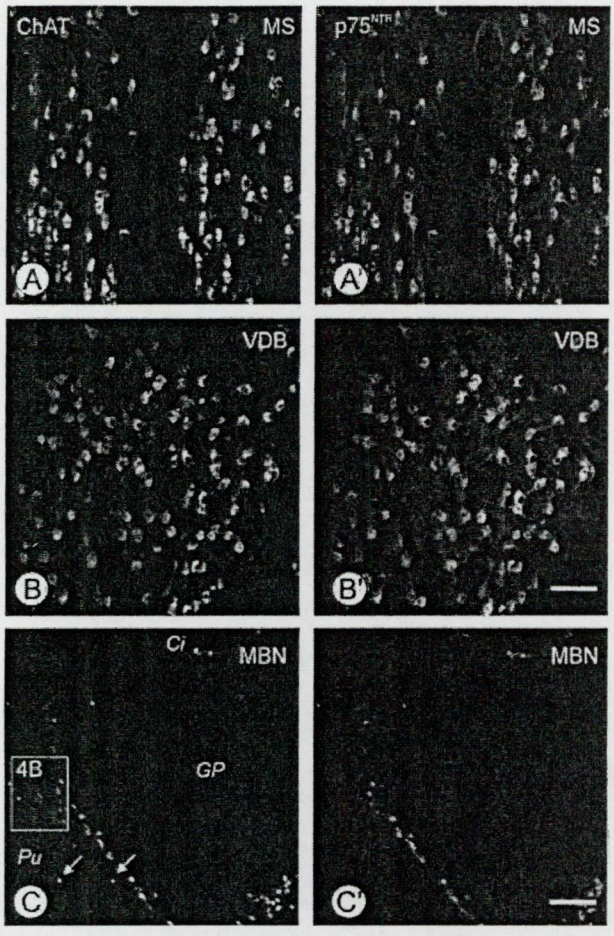

Fig. 3. Coexpression of choline acetyltransferase (ChAT; **A–C**) and low-affinity neurotrophin receptor p75 (p75^{NTR}; **A′–C′**) in the medial septum (MS), vertical diagonal band of Broca (VDB), and magnocellular nucleus basalis (MBN) as visualized by combined immunolabeling using Cy2 (green)- and Cy3 (red)-tagged secondary antibodies, respectively. Note the overlap of the two signals in the MS and VDB, the presence of cholinergic cells in the capsula interna (Ci), and the ring-like pattern of MBN neurons surrounding the globus pallidus (GP). p75^{NTR}-negative cholinergic neurons were found on the putamen (Pu)/MBN border (arrows). Box in C indicates a high magnification image of the territory shown in Figure 4B. Scale bar in B′ = 200 μm for A,B,A′,B′; bar in C′ = 500 μm for C,C′.

subdivision (Fig. 4A). The difference in p75^{NTR} immunoreactivity, thus, provides a firm basis for defining a border between the MBN and SI (Fig. 1D,D′,E,E′). Interestingly, cholinergic neurons of the posterior MBN also contained CB (Fig. 4F) and nNOS (Fig. 4I), whereas ChAT was not found in cells containing PV (Fig. 4E) or CR (data not shown).

Nucleus caudatus, putamen, and nucleus accumbens

As shown in Figure 1, the capsula interna provides structural separation between the NCa and Pu in the rabbit BFB. Although the capsula interna appears to be immunonegative for ChAT, it is often interrupted by striatal cell bridges that provide connections between the NCa and the Pu (Fig. 2F). Both the NCa and the Pu contain significant numbers of cholinergic interneurons. However, the pattern of neuronal density, as a function of the rostrocaudal axis, differs markedly (Table 2). Whereas a clearly descending anterior-to-posterior gradient in the density of ChAT-ir neurons was demonstrated in NCa, a more even distribution of cholinergic interneurons is characteristic for Pu. All cholinergic neurons of the NCa and Pu are large, round, and multipolar (Fig. 2G,H), resembling cholinergic striatal interneurons of other animal species (Sofroniew et al., 1982; Geula et al., 1993), and those situated in striatal cell bridges intruding into the capsula interna form a fusiform subset of ChAT-ir neurons (Fig. 2F). Whereas the NCa was devoid of any cellular p75^{NTR} labeling, p75^{NTR}-ir cells were found scattered in the ventromedial and laterodorsal segments of Pu (Fig. 4B). None of the other neurochemical markers (calcium-binding proteins, nNOS, TH, and SP) exhibited cellular colocalization with striatal cholinergic perikarya.

The accumbens complex could be divided into two subdivisions, by means of ChAT immunolabeling, namely, the lightly immunoreactive core and the densely stained AcSh nuclei. The core only exhibited diffuse ChAT-ir fiber staining. In contrast, AcSh not only consisted of a denser neuropil staining for ChAT but also contained, though in a relatively low density, cholinergic nerve cells (Table 2). Based on their multipolar appearance and size similarity to cholinergic neurons in Pu, these ChAT-ir nerve cells could also be regarded as cholinergic interneurons (data not shown).

Distribution of calcium-binding proteins, NOS, TH, and SP and their colocalization with cholinergic neurons

Although our primary objective was to determine whether cholinergic neuron populations coexpress the calcium-binding proteins CB, CR or PV, attention was also paid to the general distribution pattern of calcium-binding protein-containing neurons in the rabbit BFB. Relatively few CB-ir cells were localized in the midline of MS and VDB, where they were surrounded by the cholinergic cell columns or intermingled with ChAT-positive perikarya (Fig. 4C). Interestingly, CB-ir cholinergic neurons were present in the posterior MBN (Fig. 4F) but not in the anterior or intermediate MBN subdivisions. Quantitative analysis demonstrated that 19.1% ± 0.4% of cholinergic neurons in the posterior MBN subdivision exhibited CB immunoreactivity. CR-positive neuronal perikarya were also present mainly in the proximity of the MS midline. In comparison with the distribution pattern of CB-ir neurons (Fig. 4C), however, a significantly broader zone of intermingled CR-ir and ChAT-ir neurons was evident in the MS and VDB (Fig. 4D). The dorsal subdivision of the NCa and Pu exhibited intense CB and CR immunoreactivity, where both cellular and neuropil labeling for these calcium-binding proteins was present, and virtually all striatal principal neurons expressed CB. Although CR-containing cells were scattered in the rabbit VP and MBN/SI complex, numerous CR-ir passing fibers, though with heterogeneous densities, were visualized. Surprisingly, a relatively low intensity of PV-ir neuronal structures was observed in the MS and VDB relative to other

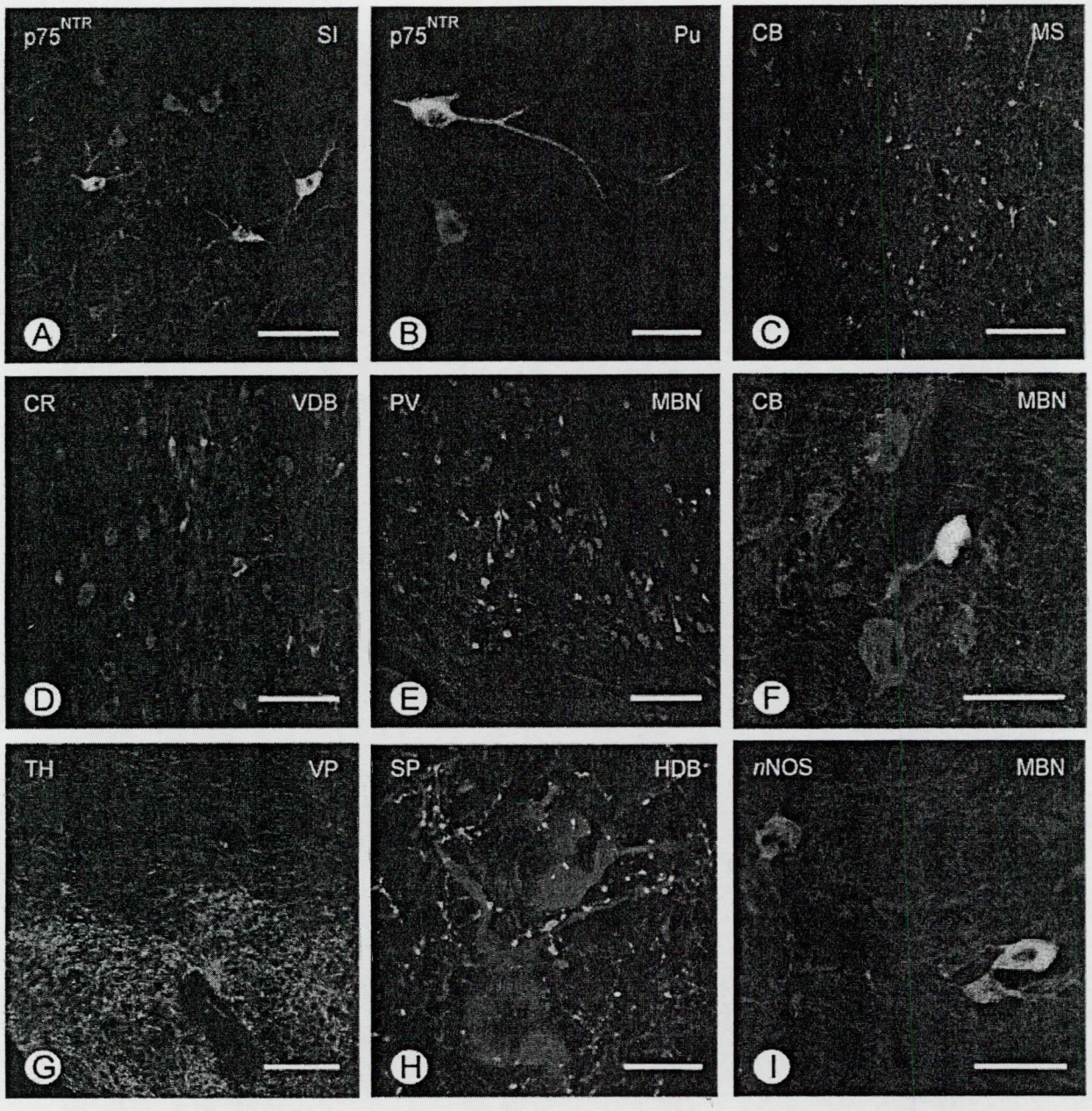

Fig. 4. Immunofluorescence labeling of choline acetyltransferase (ChAT; appears red after color coding) combined with selected neurochemical markers (color coded in green) in the rabbit basal forebrain. **A** and **B** demonstrate partial colocalization of ChAT with the low-affinity neurotrophin receptor ($p75^{NTR}$) in substantia innominata (SI) and putamen (Pu). The calcium-binding proteins calbindin D-28k (CB), calretinin (CR), and parvalbumin (PV) did not colocalize with ChAT in the medial septum (MS; **C**), vertical diagonal band of Broca (VDB; **D**), and magnocellular nucleus basalis (MBN; **E**), respectively. Interestingly, however, a portion of ChAT-immunoreactive (ir) neurons contained CB in the posterior subdivision of MBN (**F**). Low-power photomicrograph of the pallidal region (VP) depicts strong TH-positive input in the vicinity of cholinergic neurons (**G**). Also, substance P-ir fibers surround and terminate on cholinergic neurons of the horizontal diagonal band of Broca (HDB; **H**). Nitric oxide synthase (nNOS) was infrequently coexpressed in some cholinergic MBN neurons (**I**), but colocalization of nNOS with cholinergic perikarya in other investigated nuclei was not observed. Colocalization of the particular markers appears in yellow/orange. Scale bars = 100 μm in A,D, 50 μm in B,F,I, 200 μm in C,E, 250 μm in G, 20 μm in H.

BFB nuclei. In contrast, the NCa and Pu displayed a dense subset of PV-positive neurons that outnumbered the cholinergic neurons (data not shown). Similarly to the case in the MS, all three calcium-binding proteins were also present in the HDB and formed neuronal populations distinct from those of cholinergic nerve cells. Irrespective

of their particular calcium-binding protein content, noncholinergic neurons usually appeared to be smaller than cholinergic cells in rostral nuclei of the BFB. In fact, PV-ir neurons showed a wide range of somatic diameters, being largest in the GP, where they seemed to be as large as ChAT-ir neurons. Likewise, large PV-positive neurons were frequently observed in the VP and MBN/SI complex (Fig. 4E).

TH-ir projection fibers were localized in cholinergic areas that receive innervation from dopaminergic midbrain nuclei (Fig. 4G). These TH-positive fibers were of very thin appearance. Prominent TH immunosignal was present throughout the NCa and Pu as well as the AcSh. The distribution of TH-positive fiber projections was found as a distinctive marker between the AcSh and the VP, inasmuch as the VP exhibited significantly lower TH immunoreactivity, which became evident only in passing fibers (Fig. 4G). A few passing fibers were also visible in other cholinergic nuclei, such as MS, VDB, and MBN/SI complex (data not shown).

In parallel with TH-ir fibers, SP-containing projections were also found in the rabbit BFB that might originate in midbrain nuclei (Csillik et al., 1998). Similarly to the case in the rat (Bolam et al., 1986), SP-ir fibers were found predominantly in pallidal territories, whereas a lower density of SP-ir input was demonstrated in the NCa and Pu. However, other cholinergic nuclei, including the MS, HDB, and MBN, also received SPergic innervation. Interestingly, the MS was relatively weakly labeled for SP, whereas the lateral septum exhibited strong SP immunoreactivity. Similarly, cholinergic neurons in the HDB were embedded in a dense network of SP-ir fibers that seemed to form synaptic terminals on ChAT-ir neurons (Fig. 4H). In contrast to our data on TH immunoreactivity in the AcSh and VP, SP-positive fibers were abundantly present in VP, but not in AcSh, making these two markers ideal for the demarcation of these nuclei (data not shown).

nNOS-ir neurons were found only in striatal (NCa, Pu and AcSh) and pallidal (VP) subregions, where nNOS labels a group of noncholinergic small to medium-sized neurons. Other BFB nuclei were mostly devoid of nNOS immunoreactivity. Interestingly, a few cells coexpressing ChAT and nNOS were observed in the posterior MBN subterritory (Fig. 4I), with a frequency of <1%.

Cholinergic terminals in the neocortex and hippocampus

Similarly to the case in other animal species, the rabbit cerebral cortex displayed a clear laminar distribution of cholinergic projection fibers. ChAT-ir fibers formed a dense network of fine axons (Fig. 2I) with apparently highest densities in layers I and V of the cerebral cortical areas investigated. Morphometric analysis was performed on layer V of the cerebral cortex because of its clear, distinctive borders with adjacent cortical laminae and demonstrated a largely homogeneous distribution of cholinergic terminals irrespective of the particular cortical subfield investigated (Table 3). Interestingly, the adult rabbit neocortex contained only a few, faintly immunoreactive cholinergic interneurons, primarily in the somatosensory and retrosplenial areas.

Similarly, a strictly organized cholinergic fiber pattern was apparent in the dorsal hippocampus. Determination of the surface area density of cholinergic axons revealed the highest density of ChAT-ir innervation in the supra-

TABLE 3. Density of Choline Acetyltransferase (ChAT)-Immunoreactive Terminals in Cerebral Cortex and Hippocampus[1]

Brain region	Subdivision	Fiber density
Cortex	Cingulate	10.2 ± 2.6
	Retrosplenial	9.5 ± 2.2
	Somatosensory (FL)	12.0 ± 1.3
	Somatosensory (HL)	8.2 ± 1.3
	Occipital	8.1 ± 0.6
	Parietal	9.2 ± 1.9
Hippocampus	CA1 suprapyramidale	18.3 ± 1.5
	CA1 infrapyramidale	12.9 ± 1.2
	CA1 oriens	6.8 ± 0.9
	CA1 radiatum	4.6 ± 0.6
	CA3 suprapyramidale	16.8 ± 2.1
	CA3 infrapyramidale	10.6 ± 1.3
	CA3 oriens	6.4 ± 1.2
	CA3 radiatum	4.8 ± 0.6
	DG IML	11.6 ± 1.7
	DG OML	10.8 ± 2.8

[1]Distribution of ChAT-immunoreactive projections, originating in cholinergic basal forebrain nuclei, was determined in layer V of the rabbit neocortex and dorsal hippocampus. Divisions of cerebral cortical areas were identified and termed as introduced by Zilles (1985), whereas those of the dorsal hippocampus correspond to the description of Freund and Buzsáki (1996). Fiber density is presented as the mean surface area covered by skeletonized ChAT-ir projections. Data are expressed as means ± SEM. FL, forelimb representation; HL, hindlimb representation; DG IML, inner molecular layer of the dentate gyrus; DG OML, outer molecular layer of the dentate gyrus.

pyramidal layer of both the CA1 and the CA3 subfields (Fig. 2J). It is worth noting that homogeneous distribution of ChAT-ir fibers was found in the inner and outer molecular layers of the dentate gyrus (Table 3). Multipolar ChAT-ir nerve cells were frequently observed in the dorsal hippocampus (Fig. 2J).

DISCUSSION

Our report demonstrates that, as in other classes of mammals, including rodents and primates, cholinergic neurons form a confluent series of nuclei in the BFB of the rabbit, in which two classes of ChAT-ir nerve cells were identified: projection neurons of MS, VDB, HDB, and MBN/SI and interneurons of NCa, Pu, VP, whereas the GP was devoid of cholinergic cells. Projection neurons of the rabbit BFB provided dense, topologically organized innervation to the cerebral cortex and hippocampus. Interestingly, cholinergic interneurons were frequently seen in the hippocampus but were scarce in neocortical areas. Analysis of the neurochemical heterogeneity of cholinergic cell populations in rabbit BFB revealed the sparse occurrence of CB (~19%) and nNOS (<1%) in cholinergic neurons of posterior MBN, a finding that provides a phylogenetic niche for the rabbit forebrain cholinergic system between rodents (with partial nNOS coexpression; Schober et al., 1989; Brauer et al., 1991; Geula et al., 1993) and primates (with partial CB coexpression; Chang and Kuo, 1991; Côté and Parent, 1992; Geula et al., 1993; Ichitani et al., 1993; Härtig et al., 2002). This assumption is further supported by recent phylogenetic concepts indicating that the rabbit, a member of the mammalian order Lagomorpha, has a distant relationship to members of the orders of both Rodentia and Primates (Benton, 2000).

Distribution of ChAT-ir neurons

The distribution of ChAT-ir BFB projection neurons adheres well to the nomenclature introduced by Mesulam et al. (1983a, b). In particular, the rabbit MS may correspond to the "Ch1" subdivision, the VDB may be regarded as the "Ch2" cell group, and the HDB and the MBN/SI

complex can be assigned as the "Ch3" and "Ch4" regions, respectively. However, the mammalian species investigated so far exhibit marked differences in the complexity of BFB nuclei (Butcher and Semba, 1989). Increasing complexity of the BFB system, in parallel with cortical evolution, might be exemplified by the MBN. In the rat, the MBN can arbitrarily be divided into anterior, intermediate, and posterior subterritories, as was revealed by tract tracing studies (Luiten et al., 1987; Gaykema et al., 1990) that demonstrated distinct cortical projection patterns of ChAT-ir cholinergic MBN neurons. In contrast, the complexity of MBN gradually increases in primates and humans and can be subdivided into five and six subsectors, respectively (Mesulam and Geula, 1988). Here, we defined three—anterior, intermediate, and posterior—MBN subsectors based on the lack and/or presence of adjacent cholinergic nuclei and found these to be similar to those of rodents. Importantly, however, extensions of the MBN could also be observed in the lamina between the GP and the Pu, and ChAT-ir neurons coexpressing $p75^{NTR}$ in the capsula interna and adjacent to the basis of NCa could also be assumed to be parts of this nucleus (Maclean at al., 1997).

Stereology-based image analysis was used to determine the numbers of ChAT-ir nerve cells in BFB nuclei. In general terms, the total number of cholinergic neurons in rabbit BFB was approximately 37,000, ~22,000 being cholinergic projection neurons in "Ch1"–"Ch4" nuclei. To date, only a few studies have estimated the numbers of cholinergic neurons in BFB nuclei. In consideration of the findings of Smith et al. (1993, 1995) and Leanza (1998) and of Wu et al. (2000), who showed 1,000–2,000 cholinergic neurons in the rat HDB/MBN vs. approximately 55,000 ChAT-ir cells in the BFB of common marmoset, respectively, our data lend further support to the hypothesis that the complexity of the BFB cholinergic system can be regarded as a phylogenetic correlate of the differentiation of the cerebral cortex. In addition, the rabbit HDB consists of approximately the same amount of ChAT-ir cells as the MS, which is a hallmark of macrosmatic rodents (Brashear et al., 1986) and carnivores (Gritti et al., 1998), whereas the relative number of HDB cholinergic cells is much lower in the microsmatic primates (Mesulam et al., 1984). In contrast, the dorsal striatum (NCa and Pu) closely resembles that of primates, inasmuch as the capsula interna provides a clear structural separation between the two nuclei. Taken together with these data, our morphological analysis supports the theory of an increased complexity of cholinergic BFB nuclei in the rabbit compared with those of rodents (Leanza, 1998; Smith and Booze, 1995). It is likely that Old Word primates, such as apes and humans, with a large brain size, may bear even many more ChAT-ir neurons. As strict quantitative analysis of cholinergic BFB cells is as yet lacking, so accurate interspecies comparisons of absolute or relative numbers of the BFB cholinergic neurons cannot be made.

The density and distribution of cholinergic neurons in the BFB are not uniform, which is due predominantly to the alternating density of intermingled noncholinergic—primarily γ-aminobutyric acidergic—cells (Freund, 1989). For example, cholinergic neurons in the MS and VDB are situated in the midline and in compact lateral cell columns that are intermingled with noncholinergic cell populations, providing an onionskin-like structure to the nucleus (Kiss et al., 1990; Brauer et al., 1991; Jakab and Leranth, 1995). Similarly, the parallel existence of cholinergic and noncholinergic neuron populations could also be observed in the HDB and MBN/SI complex, but with considerable differences in the relative densities of cholinergic and noncholinergic nerve cells (Sarter and Bruno, 2002).

Distribution of $p75^{NTR}$-ir neurons

In the present study, a high density of $p75^{NTR}$-ir neurons was demonstrated throughout the "Ch1"–"Ch4" regions of the rabbit BFB. Double-immunofluorescence labeling experiments showed abundant colocalization of ChAT and $p75^{NTR}$ in these nuclei. Whereas virtually all cholinergic neurons expressed both markers in the MS, VDB, and HDB regions, a subpopulation of cholinergic cells located in SI was devoid of $p75^{NTR}$ immunoreactivity. We assume that these neurons correspond to $p75^{NTR}$-negative cholinergic neurons in the rat that are known to project to the amygdala (Heckers et al., 1994). It is worth noting that, in contrast to the case in the rat, the VP contains a few large cholinergic projection neurons that coexpress $p75^{NTR}$ (see also Riedel et al., 2002). Importantly, $p75^{NTR}$-ir cells without ChAT coexpression were not detectable in the rabbit BFB.

Detailed assessment of the distribution of $p75^{NTR}$-ir neurons in the BFB of the rabbit also revealed some differences from other mammalian species. For example, a unique ribbon-like distribution of large cholinergic neurons can be observed around the GP, often extending into the capsula interna. Similar, though not identical, localization of cholinergic neurons is known in mouse (Roßner et al., 2000), rat (Riopelle et al., 1987; Springer et al., 1987; Kiss et al., 1988), nonhuman primates (Riopelle et al., 1987; Wu et al., 2000), carnivores (Tremere et al., 1998, 2000), artiodactyles (Tremere et al., 2000), marsupials (our unpublished observations), and humans (Hefti et al., 1986; Mufson et al., 1989). We classified these cells as MBN-related projection neurons based on their spatial relationships to other cholinergic neurons. $p75^{NTR}$-positive cholinergic interneurons were found only in the Pu and not in the NCa, as was also described for sheep (Ferreira et al., 2001) and rat (Kokaia et al., 1998), whereas widespread distribution of $p75^{NTR}$-ir cells in the NCa, Pu, and nucleus accumbens was seen in the common marmoset (Maclean et al., 1997).

Neurochemical heterogeneity of cholinergic neurons

From a neurochemical point of view, cholinergic neurons of the rabbit BFB form a relatively homogeneous cell population. Although some cholinergic neurons coexpressed CB or nNOS in the posterior part of the MBN, colocalization of ChAT and any of the other neurochemical markers investigated was not demonstrated.

In the rat, distinct subpopulations of cholinergic projection neurons are immunoreactive for nNOS (Schober et al., 1989; Brauer et al., 1991; Geula et al., 1993). In contrast, nNOS is entirely absent in cholinergic projection cells of primates (Geula et al., 1993; Wu et al., 2000), where ChAT- and nNOS-positive neurons form nonoverlapping populations throughout the "Ch1"–"Ch4" regions. nNOS immunoreactivity is absent in cholinergic neurons of the rabbit "Ch1"–"Ch3" cell groups, although some nNOS-containing cholinergic neurons are present in the posterior MBN subdivision. It is noteworthy that this

nNOS immunoreactivity is apparently weaker than that of cortical neurons.

In the rabbit, CB expression was confined to cholinergic MBN neurons, whereas all other cholinergic cells were devoid of CB immunoreactivity. Comparative studies demonstrated that CB immunoreactivity is absent in cholinergic neurons of the rat BFB; conversely, almost all ChAT-ir neurons contain CB in the primate forebrain (Chang and Kuo 1991; Chang et al., 1991; Geula et al., 1993; Ichitani et al., 1993; Härtig et al., 2002). Moreover, Ichimiya et al. (1989) reported that CB-containing cholinergic projection neurons are first affected in Alzheimer's disease and are more severely damaged than cortical CB-ir nerve cells (Ferrer et al., 1993; Wu et al., 1997).

All BFB areas known to receive dopaminergic innervation contained strong TH-ir fiber labeling. No cell population with TH immunoreactivity was visible within the rabbit BFB. Although this finding corresponds to findings for nearly all other investigated species, TH immunoreactivity was reported in "Ch4" cholinergic cells in the common marmoset (Wisniowski et al., 1992; Wu et al., 2000).

Distribution of cholinergic terminals in the cerebral cortex and hippocampus

Similarly to the case in other mammalian species, *corticopetal and septohippocampal cholinergic projections* appear as a fine fiber network in target areas. ChAT-ir projections were present in all layers of the neocortical territories and hippocampal subfields investigated. In the cerebral cortex, the highest density of cholinergic projections was observed in layer V, followed by layers I–II = IV–VI > III. Quantitative analysis of the area density of ChAT-ir cholinergic projections in layer V, which provides information on the percentage area covered by skeletonized cholinergic fibers in a particular sampling field, demonstrated a relatively even distribution of cortical cholinergic projections, with peak density values in the FL and cingulate cortices. Interestingly, layer V of the FL and cingulate areas received the most dense cholinergic innervation also in the rat (unpublished observations), which may point to at least partial similarities in the cortical innervation of these species. Likewise, the hippocampal innervation of the rabbit also resembled that of the rat (Freund and Buzsáki, 1986), inasmuch as the CA1 and CA3 strata suprapyramidale and infrapyramidale and the inner moleculare layers and outer moleculare layers of the dentate gyrus are most abundantly covered by cholinergic fibers. Although tract tracing and electron microscopy were not performed, it seems likely that cholinergic fibers terminate on both principal and interneuron populations in the hippocampus.

From a methodological point of view, our quantitative analysis using surface area density measurements was aimed at demonstrating potential differences in the innervation density of particular projection areas, because this approach was efficiently used to record lesion-induced changes in cortical and hippocampal cholinergic innervation (Harkany et al., 2000, 2001a, b; Horvath et al., 2002). In contrast, our data, in terms of the absolute values, can be considered only as fine approximations yielded by using standard light and threshold adjustments throughout the quantification procedure.

CONCLUSIONS

The present studies provide neuroanatomical evidence of the distribution of cholinergic neurons in major BFB nuclei and their neocortical and hippocampal projections in the rabbit brain. Here we demonstrate that BFB nuclei containing cholinergic projection neurons can be subdivided into the MS, VDB, HDB, and MBN/SI complex, and their boundaries appear largely identical to those of corresponding structures in the rat. Cholinergic projection fibers formed a topologically organized network in the neocortex and hippocampus and exhibited a clear laminar distribution pattern. Overall, our data, yielded by ChAT and $p75^{NTR}$ immunocytochemistry, showed that major morphological characteristics of cholinergic corticopetal and septohippocampal magnocellular projection systems in the rabbit BFB resemble those of rodents, such as the rat and mouse. In contrast, analysis of the number and density of cholinergic neurons in BFB nuclei revealed more cholinergic neurons in the rabbit than were previously described for rodents. Moreover, double-immunofluorescence labeling of ChAT and selected neuronal markers revealed some neurochemical peculiarities, such as the limited presence of CB and nNOS in cholinergic neurons of the posterior MBN. These latter characteristics, however, can be considered as signs of the evolutionary separation of the rabbit from other mammalian species. *The neurochemical heterogeneity of MBN subdivisions* may markedly influence the sensitivity and recovery potential of cholinergic MBN neurons after noxious stimulation, which should be considered in future pharmacological models of cholinergic dysfunction in this animal species (if possible).

ACKNOWLEDGMENTS

The authors thank Mrs. Gudrun Lemm and Mrs. Ute Bauer for their technical assistance during animal handling and tissue processing, respectively.

LITERATURE CITED

Alm P, Larsson B, Ekblad E, Andersson KE. 1993. Immunohistochemical localization of peripheral nitric oxide synthase-containing nerves using antibodies raised against synthesized C- and N-terminal fragments of a cloned enzyme from rat brain. Acta Physiol Scand 148:421–429.

Armstrong DM, Saper CB, Levey AI, Wainer BH, Terry RD. 1983. Distribution of cholinergic neurons in rat brain: demonstrated by immunocytochemical localization of choline acetyltransferase. J Comp Neurol 216:53–68.

Baisden RH, Woodruff ML, Hoover DB. 1984. Cholinergic and noncholinergic septohippocampal projections: a double-label horseradish peroxidase-acetylcholinesterase study in the rabbit. Brain Res 290: 146–151.

Beach TG, Potter PE, Kuo YM, Emmerling MR, Durham RA, Webster SD, Walker DG, Sue LI, Scott S, Layne KJ, Roher AE. 2000. Cholinergic deafferentation of the rabbit cortex: a new animal model of Aβ deposition. Neurosci Lett 283:9–12.

Benton MJ. 2000. Vertebrate paleontology. Oxford: Blackwell Science.

Berger-Sweeney J, Stearns NA, Murg SL, Floerke-Nashner LR, Lappi DA, Baxter MG. 2001. Selective immunolesions of cholinergic neurons in mice: effects on neuroanatomy, neurochemistry, and behavior. J Neurosci 21:8164–8173.

Bigl V, Woolf NJ, Butcher LL. 1982. Cholinergic projections from the basal forebrain to frontal, parietal, temporal, occipital and cingulate cortices: a combined fluorescent tracer and acetylcholinesterase analysis. Brain Res Bull 8:727–749.

Bolam JP, Ingham CA, Izzo PN, Levey AI, Rye DB, Smith AD, Wainer BH. 1986. Substance P-containing terminals in synaptic contact with cho-

linergic neurons in the neostriatum and basal forebrain: a double immunocytochemical study in the rat. Brain Res 397:279–289.

Brashear HR, Záborszky L, Heimer L. 1986. Distribution of GABAergic and cholinergic neurons in the rat diagonal band. Neuroscience 17: 439–451.

Brauer K, Schober A, Wolff JR, Winkelmann E, Luppa H, Lüth H-J, Böttcher H. 1991. Morphology of neurons in the rat basal forebrain nuclei: comparison between NADPH-diaphorase histochemistry and immunohistochemistry of glutamic acid decarboxylase, choline acetyltransferase, somatostatin and parvalbumin. J Hirnforsch 32:1–17.

Brückner G, Schober W, Härtig W, Ostermann-Latif C, Webster HH, Dykes RW, Rasmusson DD, Biesold D. 1992. The basal forebrain cholinergic system in the raccoon. J Chem Neuroanat 5:441–452.

Butcher LL, Semba K. 1989. Reassessing the cholinergic basal forebrain: nomenclature schemata and concepts. Trends Neurosci 12:483–485.

Celio MR, Baier W, Schärer L, de Viragh PA, Gerday C. 1988. Monoclonal antibodies directed against the calcium-binding protein parvalbumin. Cell Calcium 9:81–86.

Celio MR, Baier W, Schärer L, Gregersen HJ, de Viragh PA, Norman AW. 1990. Monoclonal antibodies directed against the calcium binding protein calbindin D-28k. Cell Calcium 11:599–602.

Chang HT, Kuo H. 1991. Relationship of calbindin D-28k and cholinergic neurons in the nucleus basalis of Meynert of the monkey and the rat. Brain Res 549:141–145.

Chao LP, Kan KSK, Hung FM. 1982. Immunohistochemical localization of choline acetyltransferase in rabbit forebrain. Brain Res 235:65–82.

Côté PY, Parent A. 1992. Calbindin D-28k and choline acetyltransferase are expressed by different neuronal populations in pedunculopontine nucleus but not in nucleus basalis in squirrel monkeys. Brain Res 593:245–252.

Csillik B, Rakic P, Knyihár-Csillik E. 1998. Peptidergic innervation and the nicotinic acetylcholine receptor in the primate basal nucleus. Eur J Neurosci 10:573–585.

Dunnett SB, Everitt BJ, Robbins TW. 1991. The basal forebrain-cortical cholinergic system: interpreting the functional consequences of excitotoxic lesions. Trends Neurosci 14:494–501.

Eckenstein FP, Baughman RW, Quinn J. 1988. An anatomical study of cholinergic innervation on rat cerebral cortex. Neuroscience 25:457–474.

Everitt BJ, Robbins TW. 1997. Central cholinergic systems and cognition. Annu Rev Psychol 48:649–684.

Ferreira G, Meurisse M, Tillet Y, Lévy F. 2001. Distribution and colocalisation of choline acetyltransferase and p75 neurotrophin receptors in the sheep basal forebrain: implications for the use of a specific cholinergic immunotoxin. Neuroscience 104:419–439.

Ferrer I, Tunon T, Soriano E, del Rio A, Iraizoz I, Fonseca M, Guionnet N. 1993. Calbindin D-28k immunoreactivity in the temporal neocortex in patients with Alzheimer's disease. Clin Neuropathol 12:53–58.

Fleischhauer K, Zilles K, Schleicher A. 1980. A revised cytoarchitectonic map of the neocortex of the rabbit (*Oryctolagus cuniculus*). Anat Embryol 161:121–143.

Freund TF. 1989. GABAergic septohippocampal neurons contain parvalbumin. Brain Res 478:375–381.

Freund TF, Antal M. 1988. GABA-containing neurons in the septum control inhibitory interneurons in the hippocampus. Nature 336:170–173.

Freund TF, Buzsáki G. 1996. Interneurons of the hippocampus. Hippocampus 6:347–470.

Frotscher M, Vida I, Bender R. 2000. Evidence for the existence of non-GABAergic, cholinergic interneurons in the rodent hippocampus. Neuroscience 96:27–31.

Gall C. 1988. Seizures induce dramatic and distinctly different enkephalin, dynorphin, and CCK immunoreactivities in mouse hippocampal mossy fibers. J Neurosci 8:1852–1862.

Gaykema RPA. Luiten PGM, Nyakas C, Traber J. 1990. Cortical projection patterns of the medial septum-diagonal band complex. J Comp Neurol 293:103–124.

Geula C, Schatz CR, Mesulam MM. 1993. Differential localization of NADPH-diaphorase and calbindin-D28k within the cholinergic neurons of the basal forebrain, striatum and brainstem in the rat, monkey, baboon and human. Neuroscience 54:461–476.

Gritti I, Mariotti M, Mancia M. 1998. GABAergic and cholinergic basal forebrain and preoptic-anterior hypothalamic projections to the mediodorsal nucleus of the thalamus in the cat. Neuroscience 85:149–178.

Harkany T, Dijkstra IM, Oosterink BJ, Horvath KM, Ábrahám I, Keijser J, Van der Zee EA, Luiten PGM. 2000. Increased amyloid precursor protein expression and serotonergic sprouting following excitotoxic lesion of the rat magnocellular nucleus basalis: neuroprotection by Ca^{2+} antagonist nimodipine. Neuroscience 101:101–114.

Harkany T, Grosche J, Mulder J, Horvath KM, Keijser J, Hortobágyi T, Luiten PGM, Härtig W. 2001a. Short-term consequences of *N*-methyl-D-aspartate excitotoxicity in rat magnocellular nucleus basalis: effects on in vivo labelling of cholinergic neurons. Neuroscience 108:611–627.

Harkany T, Mulder J, Horvath KM, Meeberg E, Nyakas C, Luiten PGM. 2001b. Oral post-lesion administration of 5-HT_{1A} receptor agonist Repinotan hydrochloride (BAY × 3702) attenuates NMDA-induced delayed neuronal death in rat magnocellular nucleus basalis. Neuroscience 108:629–642.

Härtig W, Brückner G, Holzer M, Brauer K, Bigl V. 1995. Digoxigenylated primary antibodies for sensitive dual-peroxidase labelling of neural markers. Histochem Cell Biol 104:467–472.

Härtig W, Bauer A, Brauer K, Grosche J, Hortobágyi T, Penke B, Schliebs R, Harkany T. 2002. Functional recovery of cholinergic basal forebrain neurons under disease conditions: old problems, new solutions? Rev Neurosci 13:95–165.

Haycock JW. 1987. Stimulation-dependent phosphorylation of tyrosine hydroxylase in rat corpus striatum. Brain Res Bull 19:619–622.

Heckers S, Ohtake T, Wiley RG, Lappi DA, Geula C, Mesulam MM. 1994. Complete and selective cholinergic denervation of rat neocortex and hippocampus but not amygdala by an immunotoxin against the p75 NGF receptor. J Neurosci 14:1271–1289.

Hefti F, Hartikka J, Salvatierra A, Weiner WJ, Mash DC.1986. Localization of nerve growth factor receptors in cholinergic neurons of the human basal forebrain. Neurosci Lett 69:37–41.

Horvath KM, Härtig W, Van der Veen R, Keijser J, Mulder J, Ziegert M, Van der Zee EA, Harkany T, Luiten PGM. 2002. 17β-Estradiol enhances cortical cholinergic innervation and preserves synaptic density following excitotoxic lesions to the rat nucleus basalis magnocellularis. Neuroscience 110:489–504.

Houser CR, Crawford GD, Salvaterra PM, Vaughn JE. 1985. Immunocytochemical localization of choline acetyltransferase in rat cerebral cortex: a study of cholinergic neurons and synapses. J Comp Neurol 234:17–34.

Ichimiya Y, Emson PC, Mountjoy CQ, Lawson DE, Iizuka R. 1989. Calbindin-immunoreactive cholinergic neurones in the nucleus basalis of Meynert in Alzheimer-type dementia. Brain Res 499:402–406.

Ichitani Y, Tanaka M, Okamura H, Ibata Y. 1993. Cholinergic neurons contain calbindin-D28k in the monkey medial septal nucleus and nucleus of the diagonal band: an immunocytochemical study. Brain Res 625:328–332.

Ingham CA, Bolam JP, Wainer BH, Smith AD. 1985. A correlated light and electron microscopic study of identified cholinergic basal forebrain neurons that project to the cortex in the rat. J Comp Neurol 239:176–192.

Iraizoz I, Guijarro JL, Gonzalo LM, de Lacalle S. 1999. Neuropathological changes in the nucleus basalis correlate with clinical measures of dementia. Acta Neuropathol 98:186–196.

Jakab RL, Leranth C. 1995. Septum. In: Paxinos G, editor. The rat nervous system, 2nd ed. London: Academic Press. p 405–442.

Kan KSK, Chao LP, Eng LF. 1978. Immunohistochemical localization of choline-acetyltransferase in rabbit spinal cord and cerebellum. Brain Res 146:221–229.

Kása P. 1986. The cholinergic systems in brain and spinal cord. Prog Neurobiol 26:211–272.

Kimura H, McGeer PI, Peng JH, McGeer EG. 1981. The central cholinergic system studied by choline acetyltransferase immunohistochemistry in the cat. J Comp Neurol 200:151–201.

Kiss J, McGovern J, Patel AJ. 1988. Immunohistochemical localization of cells containing nerve growth factor receptors in the different regions of the adult rat forebrain. Neuroscience 27:731–748.

Kiss J, Patel AJ, Baimbridge KG, Freund TF. 1990. Topographical localization of neurons containing parvalbumin and choline acetyltransferase in the medial septum-diagonal band region of the rat. Neuroscience 36:61–72.

Kokaia Z, Andsberg G, Martinez-Serrano A, Lindvall O. 1998. Focal cerebral ischemia in rat induces expression of p75 neurotrophin receptor in resistant striatal cholinergic neurons. Neuroscience 84:1113–1125.

Leanza G. 1998. Chronic elevation of amyloid precursor protein expression in the neocortex and hippocampus of rats with selective cholinergic lesions. Neurosci Lett 257:53–56.

Li ZS, Furness JB. 1998. Immunohistochemical localisation of cholinergic

markers in putative intrinsic primary afferent neurons of the guinea-pig small intestine. Cell Tissue Res 294:35–43.

Luiten PGM, Gaykema RPA, Traber J, Spencer DG. 1987. Cortical projection patterns of magnocellular basal nucleus subdivisions as revealed by anterogradely transported *Phaseolus vulgaris* leucoagglutinin. Brain Res 413:229–250.

Maclean CJ, Baker FH, Fine A, Ridley RM. 1997. The distribution of p75 neurotrophin receptor-immunoreactive cells in the forebrain of the common marmoset (*Callithrix jacchus*). Brain Res Bull 43:197–208.

McGeer PL, McGeer EG, Singh VK, Chase WH. 1974. Choline acetyltransferase localization in the central nervous system by immunohistochemistry. Brain Res 81:373–379.

Mesulam MM, Geula C. 1988. Nucleus basalis (Ch4) and cortical cholinergic innervation in the human brain: observations based on the distribution of acetylcholinesterase and choline acetyltransferase. J Comp Neurol 275:216–240.

Mesulam MM, Mufson EJ, Levey AI, Wainer BH. 1983a. Cholinergic innervation of cortex by the basal forebrain: cytochemistry and cortical connections of the septal area, diagonal band nuclei, nucleus basalis (substantia innominata), and hypothalamus in the rhesus monkey. J Comp Neurol 214:170–194.

Mesulam MM, Mufson EJ, Wainer BH, Levey AI. 1983b. Central cholinergic pathways in the rat: an overview based on an alternative nomenclature (Ch1–Ch6). Neuroscience 10:1185–1201.

Mesulam MM, Mufson EJ, Levey AI, Wainer BH. 1984. Atlas of cholinergic neurons in the forebrain and upper brainstem of the macaque based on monoclonal choline acetyltransferase immunohistochemistry and acetylcholinesterase histochemistry. Neuroscience 12:669–686.

Monnier M, Gangloff H. 1961. Atlas for stereotaxic brain research on the conscious rabbit. Amsterdam: Elsevier.

Mufson EJ, Bothwell M, Lois BH, Hersh LB, Kordower JH. 1989. Nerve growth factor receptor immunoreactive profiles in the normal, aged human basal forebrain: colocalization with cholinergic neurons. J Comp Neurol 285:196–217.

Palkovits M, Magyar P, Szentágothai J. 1971. Quantitative histological analysis of the cerebellar cortex in the cat. I. Number and arrangement in space of the Purkinje cells. Brain Res 32:1–13.

Paxinos G, Watson C. 1986. The rat brain in stereotaxic coordinates. Sydney: Academic Press.

Rasmusson DD. 2000. The role of acetylcholine in cortical synaptic plasticity. Behav Brain Res 115:205–218.

Reiche D, Schemann M. 1999. Mucosa of the guinea pig gastric corpus is innervated by myenteric neurones with specific neurochemical coding and projection preferences. J Comp Neurol 410:489–502.

Riedel A, Härtig W, Seeger G, Gärtner U, Brauer K, Arendt T. 2002. Principles of rat subcortical forebrain organization: a study using histological techniques and multiple fluorescence labeling. J Chem Neuroanat 23:75–104.

Riopelle RJ, Richardson PM, Verge VMK. 1987. Distribution of nerve growth factor binding on cholinergic neurons of rat and monkey forebrain. Neurochem Res 12:923–928.

Ross AH, Grob P, Bothwell M, Elder DE, Ernst CS, Marano N, Ghrist BFD, Slemp CC, Herlyn M, Atkinson B, Koprowski H. 1984. Characterization of nerve growth factor receptor in neural crest tumors using monoclonal antibodies. Proc Natl Acad Sci USA 81:6681–6685.

Roßner S, Schliebs R, Bigl V. 2000. Intracerebroventricular infusion of CHO5, a rat monoclonal antibody directed against mouse low-affinity nerve growth factor receptor ($p75^{NTR}$), specifically labels basal forebrain cholinergic neurons in mouse brain. Metab Brain Dis 15:17–27.

Rossier J. 1981. Serum monospecificity: a prerequisite for reliable immunohistochemical localization of neuronal markers including choline acetyltransferase. Neuroscience 6:989–991.

Rye DB, Wainer BH, Mesulam MM, Mufson EJ, Saper CB. 1984. Cortical projections arising from the basal forebrain: a study of cholinergic and noncholinergic components employing combined retrograde tracing and immunohistochemical localization of choline acetyltransferase. Neuroscience 13:627–643.

Saper CB. 1984. Organization of cerebral cortical afferent systems in the rat. II. Magnocellular basal nucleus. J Comp Neurol 222:313–342.

Sarter M, Bruno JP. 1999. Abnormal regulation of corticopetal cholinergic neurons and impaired information processing in neuropsychiatric disorders. Trends Neurosci 22:67–74.

Sarter M, Bruno JP. 2002. The neglected constituent of the basal forebrain corticopetal projection system: GABAergic projections. Eur J Neurosci 15:1867–1873.

Schliebs R. 1998. Basal forebrain cholinergic dysfunction—experimental approaches and the diseased brain. Int J Dev Neurosci 16:601–613.

Schnell SA, Staines WA, Wessendorf MA. 1999. Reduction of lipofuscin-like autofluorescence in fluorescently labeled tissue. J Histochem Cytochem 47:719–730.

Schober A, Brauer K, Luppa H. 1989. Alternate coexistence of NADPH-diaphorase with choline acetyltransferase or somatostatin in the rat neostriatum and basal forebrain. Acta Histochem Cytochem 22:669–674.

Schwaller B, Buchwald P, Blümcke I, Celio MR, Hunziker W. 1993. Characterization of a polyclonal antiserum against the purified human recombinant calcium binding protein calretinin. Cell Calcium 14:639–648.

Semba K. 2000. Multiple output pathways of the basal forebrain: organisation, chemical heterogeneity, and roles in vigilance. Behav Brain Res 115:117–141.

Smith ML, Booze RM. 1995. Cholinergic and GABAergic neurons in the nucleus basalis region of young and aged rats. Neuroscience 67:679–688.

Smith ML, Deadwyler SA, Booze RM. 1993. 3-D reconstruction of the cholinergic basal forebrain system in young and aged rats. Neurobiol Aging 14:389–392.

Sofroniew MV, Eckenstein F, Thoenen H, Cuello AC. 1982. Topography of choline acetyltransferase-containing neurons in the forebrain of the rat. Neurosci Lett 33:7–12.

Sparks DL, Scheff SW, Hunsaker JC 3rd, Liu H, Landers T, Gross DR. 1994. Induction of Alzheimer-like β-amyloid immunoreactivity in the brains of rabbits with dietary cholesterol. Exp Neurol 126:88–94.

Sparks DL, Liu H, Gross DR, Scheff SW. 1995. Increased density of cortical apolipoprotein E immunoreactive neurons in rabbit brain after dietary administration of cholesterol. Neurosci Lett 187:142–144.

Sparks DL, Kuo YM, Roher A, Martin T, Lukas RJ. 2000. Alterations of Alzheimer's disease in the cholesterol-fed rabbit, including vascular inflammation. Preliminary observations. Ann N Y Acad Sci 903:335–344.

Springer JE, Koh S, Tayrien MW, Loy R. 1987. Basal forebrain magnocellular neurons stain for nerve growth factor receptor: correlation with cell bodies and effects of axotomy. J Neurosci Res 17:111–118.

Tremere LA, Brückner G, Brauer K, Rasmusson DD, Poethke R, Härtig W. 1998. Co-expression of $p75^{NTR}$- and calbindin-immunoreactivity in cholinergic neurons of the raccoon basal forebrain. Brain Res 797:351–356.

Tremere LA, Pinaud R, Grosche J, Härtig W, Rasmusson DD. 2000. Antibody for human p75 LNTR identifies cholinergic basal forebrain of non-primate species. Neuroreport 11:2177–2183.

Urban I, Richard P. 1972. A stereotaxic atlas of the New Zealand rabbit's brain. Springfield, IL: Charles C. Thomas.

West MJ. 1993. New stereological methods for counting neurons. Neurobiol Aging 14:275–285.

Winkler C, Potter A. 1911. An anatomical guide to experimental researchers on the rabbit's brain. Amsterdam: Versluys.

Wisniowski L, Ridley RM, Baker HF, Fine A. 1992. Tyrosine hydroxylase-immunoreactive neurons in the nucleus basalis of the common marmoset (*Callithrix jacchus*). J Comp Neurol 325:379–387.

Wu CK, Mesulam MM, Geula C. 1997. Age-related loss of calbindin from human basal forebrain cholinergic neurons. Neuroreport 8:2209–2213.

Wu CK, Hersh LB, Geula C. 2000. Cyto- and chemoarchitecture of basal forebrain cholinergic neurons in the common marmoset (*Callithrix jacchus*). Exp Neurol 165:306–326.

Zilles K. 1985. The cortex of the rat. Berlin: Springer Verlag.

In vivo labeling of rabbit cholinergic basal forebrain neurons with fluorochromated antibodies

Wolfgang Härtig,[CA] Csaba Varga, Johannes Kacza,[1] Jens Grosche, Johannes Seeger,[1] Paul G. M. Luiten,[2] Kurt Brauer and Tibor Harkany[2,3]

Paul Flechsig Institute for Brain Research, University of Leipzig, Jahnallee 59, D-04109 Leipzig; [1]Department of Anatomy, Histology and Embryology, University of Leipzig, An den Tierkliniken 43, D-04103 Leipzig, Germany; [2]Department of Molecular Neurobiology, University of Groningen, Kerklaan 30, NL-9750 AA Haren, The Netherlands; [3]Department of Medical Chemistry, Faculty of Medicine, University of Szeged, Szeged, Hungary

[CA]Corresponding Author

Received 2 May 2002; accepted 9 May 2002

Cholinergic basal forebrain neurons (CBFN) expressing the low-affinity neurotrophin receptor p75 ($p75^{NTR}$) were previously selectively labeled *in vivo* with carbocyanine 3 (Cy3)-tagged anti-$p75^{NTR}$, but the applied 192IgG-conjugates recognized $p75^{NTR}$ only in rat. The antibody ME 20.4 raised against human $p75^{NTR}$ had been shown to cross-react with the receptor in monkey, raccoon, sheep, cat, dog, pig and rabbit. Hence, for *in vivo* labeling of rabbit CBFN in the present study, ME 20.4 was fluorochromated with Cy3-*N*-hydroxysuccinimide ester and purified Cy3-ME 20.4 was injected intracerebroventricularly. Two days post-injection, clusters of Cy3-ME 20.4 were found in CBFN displaying choline acetyltransferase-immunoreactivity. Following photoconversion, electron microscopy revealed fluorochromated antibodies in secondary lysosomes. In conclusion, Cy3-ME 20.4 might become an appropriate marker for CBFN in live and fixed tissues of various mammalian species. *NeuroReport* 13:1395–1398 © 2002 Lippincott Williams & Wilkins.

Key words: Choline acetyltransferase; Cholinergic system; Low-affinity neurotrophin receptor; Oxygen-enriched photoconversion

INTRODUCTION

Severe damage to cholinergic neurons of the basal forebrain (BFB) is a major neuropathological hallmark of Alzheimer's disease, and this has prompted investigations focused on this brain region in various mammalian species [1]. Neuroanatomical studies have achieved the identification of cholinergic nerve cells by the detection of their marker enzyme choline acetyltransferase (ChAT, EC 3.2.1.6) as well as of vesicular acetylcholine transporters. An additional selective marker of cholinergic BFB neurons is the low-affinity neurotrophin receptor p75 ($p75^{NTR}$), as was demonstrated in the rat [2], raccoon [3], monkey [4] and human [5]. Targeting of $p75^{NTR}$ led to the development of cholinergic immunolesion models. In particular, the application of antibodies directed against an extracellular epitope of rat $p75^{NTR}$ and conjugated to the ribosome-inactivating toxin saporin (192IgG-saporin) caused selective lesions of cholinergic projection neurons in the rat BFB [6].

A further derivative of 192IgG, namely its conjugate with the red fluorochrome carbocyanine 3 (Cy3-192IgG), was introduced as a tool for the selective labeling of rat cholinergic, $p75^{NTR}$-bearing neurons both [7,8] and [9]. 192IgG-conjugates are commonly infused intracerebroventricularly and bind to $p75^{NTR}$ on cholinergic terminals, become internalized as ligand/receptor complexes and are transported retrogradely to the perikarya of cholinergic BFB neurons [6]. Internalized Cy3-192IgG molecules form clusters in secondary lysosomes [8]. Whereas ribosome inactivation by saporin causes neuronal death [6,10], Wu [11] demonstrated that pre-labeling of cholinergic neurons with Cy3-192IgG does not alter their electrophysiological and pharmacological properties in brain slice preparations containing the medial septum/diagonal band complex (MSDB). Concordantly, identification of cholinergic nerve cells with Cy3-192IgG in brain slices led to new insights in the synaptic organization of neurons in the MSDB with implications for learning and memory [11,12].

However, 192IgG conjugates recognize $p75^{NTR}$ only in the rat precluding their application in other mammalian species (e.g. monkeys) with a BFB chemoarchitecture resembling that in humans [13]. In contrast, the monoclonal antibody ME 20.4 raised against an extracellular epitope of the human $p75^{NTR}$ [14] was demonstrated to cross-react with $p75^{NTR}$ also in monkey, raccoon [3], rabbit, pig, dog and cat [15]. Accordingly, the ME 20.4-saporin conjugate was shown to be a selective cholinotoxin in the common marmoset [16], rhesus monkey [17], rabbit [18] and sheep [19].

To overcome the restriction of labeling in the rat, the present study investigated whether Cy3-ME 20.4 can be employed as a marker of living cholinergic neurons in a wide range of mammalian species expressing analogues of the human $p75^{NTR}$. Encouraged by recent data on ME 20.4-saporin-induced immunolesions of cholinergic cells and

subsequent β-amyloid deposition in the rabbit brain [18], the potential of Cy3-ME 20.4 as a label for cholinergic nerve cells was exemplified in studies on BFB neurons of this animal species.

MATERIALS AND METHODS

Preparation of Cy3-ME 20.4: Cy3-ME 20.4 was prepared by coupling the antibody with a chemically activated ester of Cy3 under reaction conditions proved to maintain the antigen-binding properties of ME 20.4 [20]. Four hundred micrograms of ME 20.4 (pure IgG; AB-N07, Advanced Targeting Systems, San Diego, CA, USA) were reacted with a monofunctional Cy3-Ò-hydroxysuccinimide ester (Antibody Cy3 Labeling Kit, Amersham Pharmacia Biotech, Freiburg, Germany) according to the instruction of the manufacturer at pH 9.3 for 1 h, but with doubled dye:protein ratio. Thereafter, the reaction mixture was dialyzed against phosphate-buffered saline (3 × 4 h) and the concentration of Cy3-ME 20.4 was adjusted to approximately 0.5 mg/ml prior its use for intracerebroventricular (i.c.v.) injections.

Surgical procedure: New Zealand white rabbits of either sex (² = 5; 2.3–5.1 kg; 4–21 months of age) were used in this study. The rabbits were anesthetized with a mixture of ketamine (50 mg/kg; Exalgon, Merck, Hallbergmoos, Germany) and xylazine (4 mg/kg; Rompun, Bayer AG, Leverkusen, Germany), and their heads were mounted in a stereotaxic frame. Two animals received unilateral i.c.v. injections, and three animals were injected bilaterally with 16 µl Cy3-ME 20.4 at an infusion speed of 0.5 µl/min with a Hamilton microsyringe (Hamilton, Bonaduz, Switzerland). Injection co-ordinates were applied according to Beach »¬¿ô [18] at AP = 0.0 mm, L = 2.2 mm and DV = 9.0/7.5 mm relative to bregma. All efforts were made to minimize animal suffering throughout the experiments including administration of the analgetic Metamizol (150 mg/kg; Berlosin, Berlin-Chemie, Germany) immediately after operation. The antibiotic Enrofloxacin (10 mg/kg daily; Baytril, Bayer AG) was given orally throughout the post-injection period. The care and treatment of the animals were in accordance with the European Communities Council Directive (86/609/EEC) and approved by the Laboratory Animal Care and Use Committee of the University of Leipzig (TVV-Nr.15/00).

Immunocytochemistry and electron microscopy: Two days post-injection rabbits were transcardially perfused with 4% paraformaldehyde containing either 0.5% glutardialdehyde (three animals) or 0.1% glutardialdehyde (two animals) in 0.1 M phosphate-buffer (pH 7.4). Whole brains were removed from the skulls, divided into fore- and hindbrain regions and post-fixed overnight in 4% paraformaldehyde. Two forebrains were coronally sectioned on a vibratome at 50 µm and the remaining tissue was cryoprotected and cut at 30 µm on a cryostat microtome. Sections spanning the MSDB and the anterior subdivision of the nucleus basalis magnocellularis were washed with Tris-buffered saline (TBS, 0.1 M, pH 7.4), rinsed in distilled water, mounted, air-dried and coverslipped with Entellan (in toluene; Merck, Darmstadt, Germany).

To determine the specificity of · ² ª· ª labeling, Cy3-ME 20.4 pre-labeled sections were applied to the concomitant immunolabeling of ChAT and the calcium-binding protein calretinin. Non-specific binding sites for the immunoreagents were primarily blocked with 5% normal donkey serum in 0.1 M Tris-buffered saline (TBS) containing 0.3% Triton X-100 for 1 h. Subsequently, the sections were incubated with a mixture of affinity-purified goat anti-ChAT (1:25; AB144P, Chemicon International; Hofheim, Germany) and rabbit anti-calretinin (1:300; AB149, Chemicon) diluted in the blocking solution for 16 h. Next, rinsed sections were reacted with a cocktail of Cy2-tagged donkey anti-goat IgG and Cy5-conjugated donkey anti-rabbit IgG (20 µg/ml; Dianova, Hamburg, Germany) diluted in TBS containing 2% bovine serum albumin for 1 h. Omission of the primary antibodies in control experiments led to the absence of any cellular Cy2- and Cy5-labeling. After the cytochemical procedures the sections were rinsed, mounted, air-dried and coverslipped in Entellan. Fluorescence microscopy was performed using an Axioplan microscope (Zeiss, Oberkochen, Germany) and selected sections were inspected with a Zeiss 510 confocal laser-scanning microscope.

To quench the autofluorescence caused by lipophilic lipofuscin-like compounds in sections from 21-month-old rabbits, tissue was treated with Sudan Black B according to Schnell »¬¿ô [21] but prior to the immunofluorescence labeling of cholinergic neurons. All Sudan Black B-pretreated sections were embedded in glycerol/gelatin (Sigma, Deisenhofen, Germany).

The subcellular distribution of Cy3-ME 20.4 was determined following photoconversion of Cy3-ME 20.4 into an electron-dense reaction product applying oxygen-enriched photoconversion in a closed conversion chamber as described previously [8]. Specimens were analyzed with a Zeiss 900 electron microscope.

RESULTS

Two days following the i.c.v. infusion of Cy3-ME 20.4 there was strong punctate labeling in many cells of the MSDB (Fig. 1) that became less intense in the nucleus basalis magnocellularis. This staining pattern was observed irrespective of the concentration of glutardialdehyde in the fixative. In comparison to rabbits unilaterally infused with Cy2-ME 20.4, bilaterally injected animals appeared to contain more · ² ª· ª labeled nerve cells in both hemispheres.

· ² ª· ª labeling of Cy3-ME 20.4 was exclusively found in cholinergic neurons, as revealed by their immunoreactivity for ChAT (Fig. 1a) and $p75^{NTR}$ (not shown). In contrast, · ² ª· ª labeling was never observed in non-cholinergic, calretinin-immunoreactive nerve cells (Fig. 1b) that are known to be intermingled with cholinergic neurons in the border zone of the medial and lateral septum [22] and in magnocellular, parvalbumin-containing GABAergic BFB neurons (not shown).

It is noteworthy that treatment of the sections from 21-month-old rabbits with Sudan Black B quenched the autofluorescence caused by lipophilic lipofuscin-like compounds. Importantly, Sudan Black B treatment only slightly diminished the intensity of · ² ª· ª labeling with hydrophilic

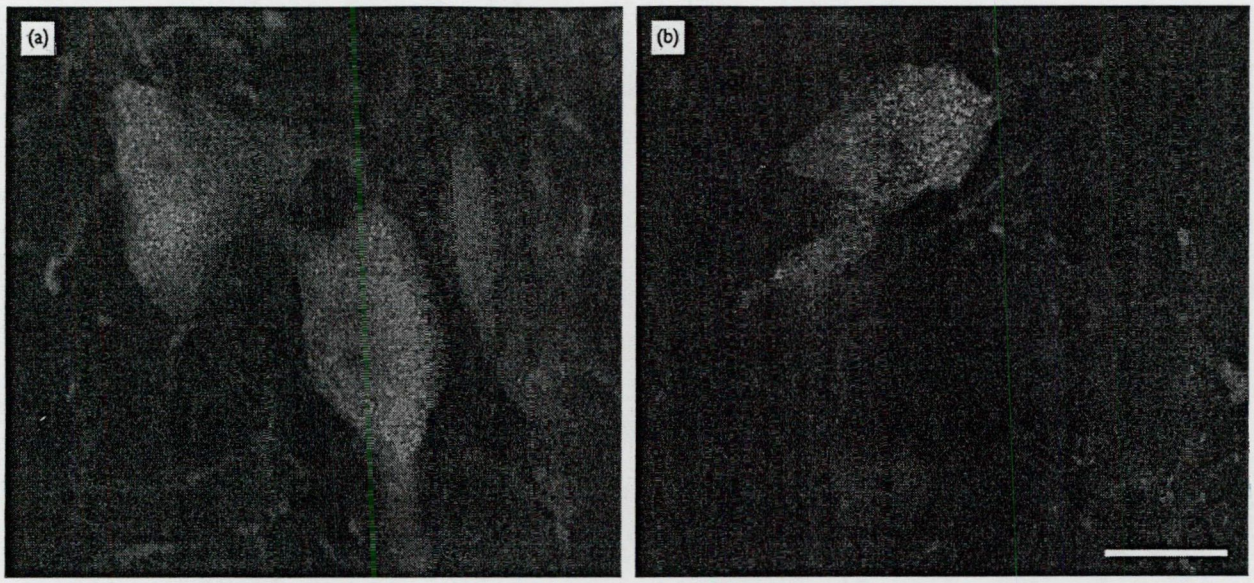

Fig. 1. The confocal laser-scanning micrograph (**a**) shows red punctate Cy3-ME 20.4 *in vivo* labeling in cholinergic neurons of the rabbit medial septum. Selectivity of Cy3-ME 20.4 for cholinergic neurons was demonstrated by co-localization with choline acetyltransferase (ChAT) that appears green (Cy2). (**b**) Merged carbocyanine triple fluorescence staining of Cy3-ME 20.4 (red clusters) and immunoreactivities for ChAT (Cy2, green) and calretinin (Cy5, color-coded in blue) in the border zone between the medial and lateral septum confirmed the specificity of *in vivo* labeling for cholinergic neurons and its absence in non-cholinergic, calretinin-containing nerve cells. Bar = 25 μm.

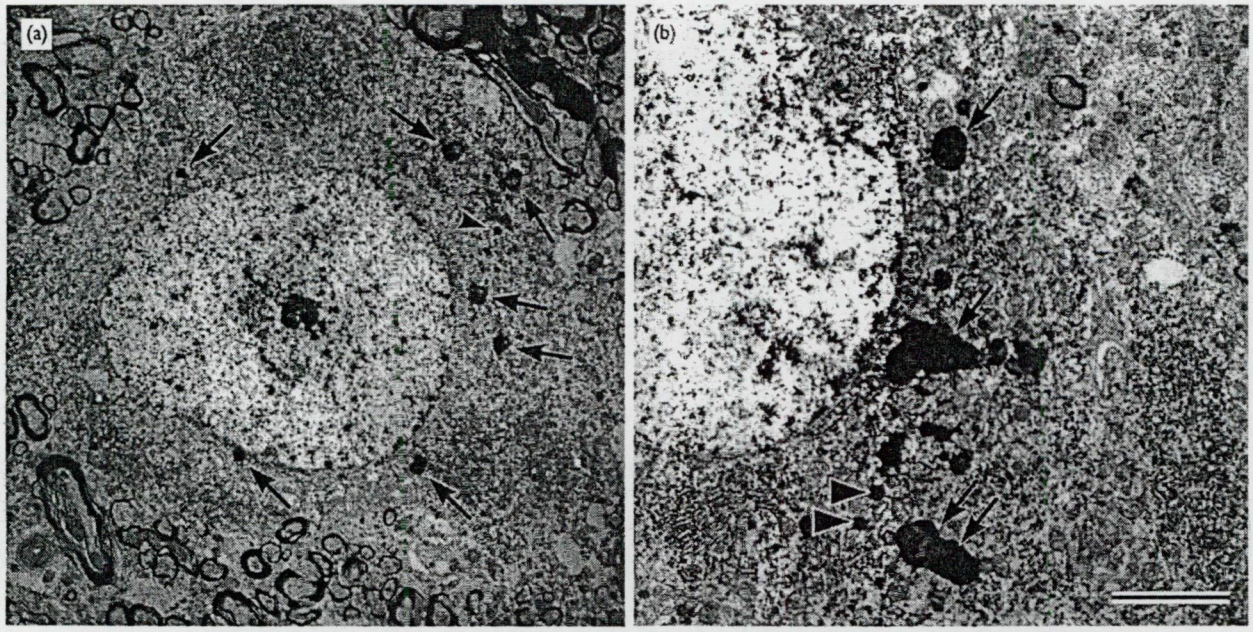

Fig. 2. Electron micrographs of cholinergic neurons in the medial septum (**a**) and, at higher magnification, in the diagonal band of Broca (**b**) following photoconversion of internalized Cy3-ME 20.4. The *in vivo* label was predominantly present in secondary lysosomes (arrows) after two days of survival. In comparison to the photoconverted material, non-labeled primary lysosomes (arrowheads) are different in their size, shape and electron density. Prior to print, the brightness and contrast of the electron micrographic images were digitally adjusted and shading correction was performed to reduce the effects of uneven illumination. Bar = 500 nm (a), 250 nm (b).

Cy3 and of the subsequently performed Cy2-immunostaining of cholinergic neurons.

Electron microscopic analysis elucidated that Cy3-ME 20.4 was predominantly located intracellularly in secondary lysosomes (Fig. 2a,b).

DISCUSSION

The granular cellular labeling of neurons in the rabbit BFB with i.c.v. applied Cy3-ME 20.4 resembled that of Cy3-192IgG in the rat BFB [7]. A subpopulation of cholinergic neurons in the MSDB was unlabeled by Cy3-ME 20.4 that also parallels the incomplete Cy3-192IgG labeling in the rat [7,11]. Recently, the counting of Cy3-192IgG-positive cells in the rat BFB revealed a medial septum ≥ horizontal limb of the diagonal band > > nucleus basalis magnocellularis gradient of labeling efficacy [23]. An apparently similar gradient was observed after the · ² ª· ª labeling with Cy3-ME 20.4; that, however, remains to be quantified. Future studies should also elucidate whether the · ² ª· ª labeling with Cy3-ME 20.4 is long-term stable or undergoes gradual clearance from the neurons, as was previously shown for Cy3-192IgG in the rat [8].

The predominant location of Cy3-ME 20.4 in secondary lysosomes, as revealed by electron microscopy, is identical to the ultrastructural localization of Cy3-192IgG in rat basal forebrain neurons [8]. This finding also corresponds with the observation that lysosomes are preferred targets for internalized nerve growth factor [24], the natural ligand of $p75^{NTR}$, which might be mimicked by fluorochromated antibodies raised against $p75^{NTR}$.

Whereas the quenching of autofluorescence with Sudan Black B in the present work hardly affected the intensity of · ² ª· ª labeling and subsequent immunofluorescence staining, strong autofluorescence might interfere with the identification of cholinergic neurons with Cy3-ME 20.4 in live brain slices originating from aged animals.

Our present findings suggest the potential use of Cy3-ME 20.4 in future neuropharmacological studies targeting the cholinergic system of higher mammals. Such investigations are also emphasized by the accelerated gathering of pharmacological data based on the · ² ª· ª labeling of rat cholinergic basal forebrain neurons [11,12]. In particular, these studies showed that muscarinic receptor antagonists induce memory impairment due to a decrease of septo-hippocampal GABA release, instead of the previously assumed diminished hippocampal acetylcholine release, and confirmed neuroanatomical data on collaterals of cholinergic neurons contacting parvalbumin-immunopositive GABAergic neurons within the MSDB [25].

CONCLUSION

The high interspecies variability of the chemical nature, structure and topography of the cholinergic components in magnocellular BFB nuclei hampers the development of general functional concepts based on investigations of only one or a few animal species. Therefore, the use of ME 20.4-saporin conjugates both in primates [16,17] and in sheep [19] suggests that Cy3-ME 20.4 might be successfully employed also in primates and ungulates, and become a useful cholinergic marker to determine morphological, electrophysiological and pharmacological parameters of cholinergic neurons under physiological or pathological conditions.

REFERENCES

1. Záborszky L, Pang K, Somogyi J »¬¿ð ß²² ÒÇ ß ⅛¼Í ½ **77**, 339–367 (1999).
2. Springer JE, Koh S, Tayrien MW and Loy R. ÖÒ»«®±½ Î »-**17**, 111–118 (1987).
3. Tremere L, Brückner G, Brauer K »¬¿ðÞ®¿· ² Î »-**797**, 351–356 (1998).
4. Kordower JH, Bartus RT, Bothwell M »¬¿ðÖÝ± ° Ò»«®± **277**, 465–486 (1988).
5. Hefti F, Hartikka J, Salvaterra P »¬¿ðÒ»«®±½ Ô-¬**69**, 275–281 (1986).
6. Wiley RG. Ì®² ¼ Ò»«®±½ **15**, 285–290 (1992).
7. Härtig W, Seeger J, Naumann T »¬¿ðÞ®¿· ² Î »-**808**, 155–165 (1998).
8. Kacza J, Grosche J, Seeger J »¬¿ðÞ®¿· ² Î »-**867**, 232–238 (2000).
9. Ha DH, Robertson RT and Weiss JH. ÖÒ»«®±½ **18**, 4201–4215 (1998).
10. Rossner S. ¬ÖÜ»ª Ò»«®±½ **15**, 835–850 (1997).
11. Wu M, Shanabrough M, Leranth C and Alreja M. ÖÒ»«®±½ **20**, 3900–3908 (2000).
12. Alreja M, Wu M, Liu W »¬¿ðÖÒ»«®±½ **20**, 8103–8110 (2000).
13. Geula C, Schatz C-R and Mesulam M-M. Ò»«®±½»²¼ **54**, 461–476 (1993).
14. Ross AH, Grob P, Bothwell M »¬¿ðÐ®±/Ò¿¬ß ⅛¼Í ½ ËÍß **81**, 6681–6685 (1984).
15. Tremere LA, Pinaud R, Grosche J »¬¿ð Ò»«®±°± ¬**11**, 2177–2183 (2000).
16. Fine A, Hoyle C, Maclean CJ »¬¿ðÒ»«®±½»² ¼**81**, 331–343 (1997).
17. Mrzljak L, Levey A, Belcher S and Goldman-Rakic PS. ÖÝ± ° Ò»«®±**390**, 112–132 (1998).
18. Beach TG, Potter PE, Kuo Y-M »¬¿ðÒ»«®±½ Ô-¬**283**, 9–12 (2000).
19. Fereira G, Meurisse M, Tillet Y and Lévy F. Ò»«®±½»² ¼**104**, 419–439 (2001).
20. Härtig W and Fritschy J-M. Immunofluorescence: conjugation of dyes to antibodies. In: Û³ ¼Ý§ ± · ½Û² ⅛½±»¼ ¿ ± Ô ° Í ½»² ¼-ondon: Nature Publishing Group; 2000. www.els.nat, pp. 1–3.
21. Schnell SA, Staines WA and Wessendorf MW. ÖØ· - ¬½»³ Ý§¬½»³ **47**, 719–730 (1999).
22. Jakab RL and Leranth C. Septum. In: Paxinos G, ed. Ì ·» Î ¿¬Ò»«® ± - Í §- ¬³ ðLondon: Academic Press; 1995, pp. 405–442.
23. Harkany T, Grosche J, Mulder J »¬¿ðÒ»«®±½»² ¼**108**, 611–627 (2001).
24. Kasaian MT and Neet KE. ÖÞ· ± Ý·» ³ **263**, 5083–5090 (1988).
25. Brauer K, Seeger G, Härtig W »¬¿ðÖÒ»«®±½ Î »-**54**, 248–253 (1998).

Acknowledgements: The excellent technical assistance of Mrs Ute Bauer, Mrs Gabriele Lindner and Mrs Gudrun Lemm is gratefully acknowledged. This study was supported by the Deutsche Forschungsgemeinschaft (grant Ha 2211/2-1 to W.H. and C.V.), the Interdisziplinäres Zentrum für Klinische Forschung (IZKF) at Leipzig University (grant 01 KS 9504 projects Z10 and C5 to J.G. and J.S., respectively) and the Hungarian National Science Foundation (OTKA, F035254, to T.H.).

Distinct subsets of nucleus basalis neurons exhibit similar sensitivity to excitotoxicity

Tibor Harkany,[1,2,6] Csaba Varga,[3,4] Jens Grosche,[3] Jan Mulder,[1] Paul G. M. Luiten,[1] Tibor Hortobágyi,[5] Botond Penke[2] and Wolfgang Härtig[3,CA]

[1]Department of Molecular Neurobiology, University of Groningen, The Netherlands; Departments of [2]Medical Chemistry and [5]Pathology, University of Szeged, Szeged, Hungary, [3]Paul Flechsig Institute for Brain Research, University of Leipzig, Leipzig, Germany, [4]Laboratory of Molecular Neurobiology, Biological Research Center of the Hungarian Academy of Sciences, Szeged, Hungary
[6]Present and corresponding Address: Unit of Molecular Neurobiology, Department of Medical Biochemistry and Biophysics, Scheeles väg 1:A1, Karolinska Institute, S-171 77 Stockholm, Sweden

[CA]Corresponding Author

Received 30 December 2001; accepted 15 February 2002

Excitotoxic lesions in the magnocellular nucleus basalis (MBN) lead to a significant damage of cholinergic neurons concomitant with increased amyloid precursor protein (APP) expression in the cerebral cortex. However, the sensitivity of non-cholinergic neurons to excitotoxicity, and changes of APP expression in the damaged MBN are still elusive. Hence, we performed multiple-labeling immunocytochemistry for choline-acetyltransferase (ChAT), neuron-specific nuclear protein (NeuN) and APP 4, 24, and 48 h after NMDA infusion in the MBN. Whereas all cholinergic neurons were immunoreactive for NeuN, this neuronal marker also labeled a population of ChAT-immunonegative non-cholinergic neurons. Both neuron populations exhibited a similar degree of sensitivity to NMDA excitotoxicity that became evident as early as 4 h post-lesion. Cholinergic MBN neurons showed abundant APP immunoreactivity (~90%), while only a fraction (~20–30%) of non-cholinergic neurons expressed the protein. Remarkably, cholinergic but not non-cholinergic neurons retained their APP immunoreactivity after NMDA infusion. In conclusion, cholinergic MBN neurons are not preferentially sensitive to short-term excitotoxicity, but are one of the major sources of APP in the basal forebrain. *NeuroReport* 13:767–772 © 2002 Lippincott Williams & Wilkins.

Key words: Basal forebrain; Choline-acetyltransferase; Confocal laser scanning microscopy; Excitotoxicity; *In vivo* labeling; Neurodegeneration; Neuron-specific nuclear protein; Rat

INTRODUCTION

The basal forebrain (BF) complex of mammals consists of a confluent series of neuron populations that are anatomically subdivided in the medial septum, diagonal bands of Broca, and the magnocellular nucleus basalis (MBN) [1]. Whereas BF neurons are substantially interconnected and form a diffuse neuronal network, their projections show a topologically defined distribution pattern with major output pathways to the hippocampus and cerebral cortex [2,3]. BF neurons exhibit a variety of neurotransmitter phenotypes, including magnocellular cholinergic, Ca^{2+}-binding protein (CaBP)-containing GABAergic, glutamatergic and neuropeptidergic neurons [2,4,5]. The complex chemical neuroanatomy of the BF correlates with the diversity of brain functions these neurons modulate.

Cholinergic BF neurons are critically involved in the modulation of learning and memory processing, and are among the severely affected neuron populations in Alzheimer's disease (AD) [6,7]. Hence, the vast majority of recent neuropharmacological investigations focused on the sensitivity, temporal profile of degeneration and eventual rescue of cholinergic BF neurons and their projections following noxious stimulation [7,8]. Cholinergic BF neurons were shown to be highly sensitive to excitotoxicity as was indicated by a robust loss of their marker enzyme choline-acetyltransferase (ChAT) [9,10], while their survival was significantly enhanced by multiple neuroprotective compounds [8,10,11]. In contrast, little is known about the reactivity of subpopulations of non-cholinergic BF neurons to neurotoxic insults. Although particular attention was directed towards the identification of a role for CaBPs in GABAergic interneurons, that may serve as a potential means to rescue nerve cells from Ca^{2+} overload associated with acute excitotoxicity [12,13], data are lacking as to whether acute excitotoxicity affects other non-cholinergic neuron populations in the BF complex.

A central though still unresolved question in the pathogenesis of AD is the relationship of cholinergic breakdown and altered expression of the amyloid precursor protein (APP). Previous studies demonstrated that lesions to

BF nuclei elicit a rapid and persistent increase of APP expression in the cerebral cortex [14–16]. However, these studies solely focused on the temporal profile of APP expression and its cholinergic modulation in the cerebral cortex.

Taking the above data together, in the present study we determined the number of cholinergic and non-cholinergic neurons using multiple-labeling immunocytochemistry under control conditions as well as 4, 24 and 48 h after NMDA infusion in the MBN. Cholinergic neurons were identified by their immunoreactivity for ChAT and by *in vivo* labeling employing the fluorochromated anti-p75 low-affinity neurotrophin receptor antibody, carbocyanine 3 (Cy3)-192IgG [9,17,18]. Neuron-specific nuclear protein (NeuN) was introduced as a pan-neuronal marker [19] to visualize neuronal perikarya irrespective of their neurotransmitter contents in the MBN. Moreover, APP immunoreactivity of the nerve cell populations, and its temporal changes under excitotoxic conditions were also investigated.

MATERIALS AND METHODS

In vivo labeling: Young adult male Wistar rats (250–300 g, $n = 12$; $n = 4$/group; bred at the University of Groningen) were caged individually and kept on a normal laboratory diet and tap water *ad lib*. All efforts were made to minimize animal suffering throughout the experiments. Their care and treatment were in accordance with the directives of the Local Ethical Committee of the University of Groningen (DEC 2493/2000). The rats were deeply anesthetized with isoflurane (2.0% (v/v%) in 70% N_2O/30% O_2; 1.5 l/min flow rate) and their head position was secured in a stereotaxic frame (Narishige International, London, UK). For the *in vivo* labeling of BF cholinergic neurons 5 µl Cy3-192IgG (~1 mg/ml in phosphate-buffered saline [PBS] 0.01 M, pH = 7.4) were injected slowly (0.5 µl/min) into the right lateral ventricle (AP −1 mm; L 1.5 mm; DV 3.2 mm) [20] with a Hamilton microsyringe. Cy3-192IgG was prepared by fluorochromation of pure 192IgG (3.5 mg/ml, containing no additives; Dianova, Hamburg, Germany) with Cy3-*N*-hydroxysuccinimide ester using a FluoroLink-Antibody Cy3 Labeling Kit (Amersham Pharmacia Biotech., Freiburg, Germany), as described recently in detail [9].

NMDA infusion in MBN: Previous studies demonstrated that application of Cy3-192IgG does not alter either the electrophysiological or neurochemical properties of cholinergic neurons [9,17,18]. Therefore, 24 h later the rats were re-anesthetized with isoflurane, fixed in the stereotaxic apparatus and 1 µl NMDA (60 mM; Sigma, St. Louis, MO, USA) was injected in the right MBN (AP −1.5 mm; L 3.2 mm; DV 6.5 mm) [20] at an infusion rate of 0.1 µl/min [9]. NMDA was freshly dissolved in PBS. As dissolving of NMDA considerably decreases the pH value of its vehicle, pH equivalent PBS (1 µl; pH = 4.0) was used as control and injected in the contralateral (left) MBN of each animal in a manner identical to the NMDA infusion procedure. Short-term effects of NMDA infusion on MBN neurons were studied after a post-lesion delay of 4, 24, and 48 h.

Immunocytochemical procedures: Fixation of the brains was carried out under deep sodium pentobarbital anesthesia by transcardial perfusion with 350 ml fixative composed of 4% paraformaldehyde in 0.1 M phosphate buffer (PB, pH 7.4), which was preceded by a short pre-rinse (50 ml) with ice-cold physiological saline. Brains were post-fixed for 2 h in the same fixative and subsequently cryoprotected by overnight storage in 30% sucrose in PB at 4°C. Coronal sections were cut on a cryostat microtome at a 30 µm thickness and collected in PBS containing 0.1% sodium azide.

Immunofluorescence labeling of APP, ChAT and NeuN was performed simultaneously on free-floating sections from all animals. All procedures started with extensive rinsing of the sections with 0.1 M Tris-buffered saline (TBS; pH 7.4) followed by blocking of non-specific binding sites for the subsequently applied immunoreagents with 10% normal donkey serum and 2% bovine serum albumin (BSA) in TBS containing 0.3% Triton X-100 (blocking solution; BS) for 1 h at room temperature. A first series of sections was double-stained for APP and NeuN by incubating the tissue in a mixture of goat anti-APP (1:40, raised against the amino acid sequence 45–62 of APP; AB 1593, Chemicon, Hofheim, Germany; according to [10]) and mouse anti-NeuN (1:100, MAB 377, Chemicon; [19]) primary antibodies in BS for 20 h. This was followed by the concomitant processing of the tissue with Cy2-conjugated donkey anti-goat and Cy3-tagged donkey anti-mouse IgG. Both antibodies, as also all other highly purified fluorochromate immunoreagents applied in this study, were obtained from Dianova (Hamburg, Germany) as supplier for Jackson ImmunoResearch (West Grove, PA, USA), and used at a concentration of 20 µg/ml in TBS containing 2% BSA (TBS-BSA) for 1 h at room temperature. In parallel, double labeling for ChAT and NeuN, as well as for ChAT and APP was performed employing rabbit anti-ChAT (1:400; AB 143, Chemicon) [9,17], mouse anti-NeuN (1:50) and goat anti-APP (1:20) primary antibodies that were diluted in BS and incubated overnight. Immunoreactivities were then visualized by applying appropriate mixtures of Cy3-conjugated donkey anti-rabbit IgG, Cy2-donkey anti-mouse IgG, or Cy2-donkey anti-goat IgG. Detection of NeuN as above was also combined with the red fluorescent immunostaining of ChAT, which stained all cholinergic neurons including those pre-labeled by Cy3-192IgG, and of APP. The sections were primarily incubated in a mixture of mouse anti-NeuN (1:50), rabbit anti-ChAT (1:400) and goat anti-APP (1:20) in BS overnight. Next, the immunoreactivities were revealed by applying a mixture of 7-amino-4-methylcoumarin-3-acetyl (AMCA)-tagged donkey anti-goat IgG (30 µg/ml), Cy3-conjugated donkey anti-rabbit IgG and Cy2-coupled donkey anti-mouse IgG in TBS-BSA for 1 h. For the quadruple staining of Cy3-192IgG, ChAT, APP and NeuN, sections were exposed to a mixture of rabbit anti-ChAT (1:100), goat anti-APP (1:40) and mouse anti-NeuN (1:50) antibodies diluted in BS overnight. Extensively rinsed tissue was then reacted with a cocktail composed of AMCA-conjugated donkey anti-rabbit IgG (30–40 µg/ml; TBS-BSA), Cy5-tagged donkey anti-goat IgG and Cy2-coupled donkey anti-mouse IgG for 1 h. In control experiments, omission of the primary antibodies yielded absence of any cellular labeling. Additional control experiments were performed

by switching the fluorophores related to the relevant cytochemical markers to confirm their labeling patterns. After all immunocytochemical procedures the sections were extensively rinsed in TBS, dipped in distilled water, mounted and coverslipped with Entellan (in toluene, Merck, Darmstadt, Germany).

Quantification and statistical analysis: At least three sections spanning the intermediate MBN in each animal were used to investigate the effects of vehicle and NMDA infusions. The number of all immunoreactive neurons was determined in both the ipsilateral and contralateral MBN as described previously in detail [9]. Care was given not to include fragmented neuronal profiles. Total cell numbers for ChAT and NeuN were estimated using the disector formula as described elsewhere [21]. The degree of co-localization of selected pairs of markers was determined in a semi-quantitative fashion. To this end, double- or triple-labeled sections were employed and inspected using a Zeiss Axioplan fluorescence microscope equipped with appropriate double and triple band pass filters (Zeiss, Jena, Germany). Representative triple and quadruple-labeled sections were imaged with an LSM 510 confocal laser-scanning microscope (Zeiss).

The effect of NMDA lesions on the number of neurons, as well as on the degree of co-localization of the cellular markers at the particular post-lesion time points was statistically evaluated using paired *t*-test (SPSS for Windows, release 10.0, SPSS Inc., Chicago, IL, USA). Significance was defined as an overall effect on the entire MBN region sampled. $p < 0.05$ was taken as indicative of statistical significance. Data were expressed as percentages and presented as means $\pm$ s.e.m.

RESULTS

Under control conditions, ChAT-immunoreactive (ir) magnocellular neurons formed the well-known neuronal network in the MBN (Fig. 1a, Fig. 2a), and were frequently *in vivo* labeled with Cy3-192IgG (Fig. 1b) [9]. Quantitative analysis of ChAT-ir nerve cells 4, 24, and 48 h after vehicle infusion in the MBN revealed 2167 $\pm$ 383, 2531 $\pm$ 109 and 2618 $\pm$ 294 neurons, respectively. All ChAT-positive neurons also displayed NeuN immunoreactivity (Fig. 1b, Fig. 2a). In contrast, only ~50% of NeuN-positive nerve cells were also immunoreactive for ChAT (Table 1). Thus, the population of NeuN-ir but ChAT-immunonegative MBN neurons corresponds with intermingled non-cholinergic neurons in the MBN. Accordingly, estimation of the number of NeuN-positive neurons in the sham-lesioned MBN indicated 4541 $\pm$ 434, 4441 $\pm$ 351 and 5071 $\pm$ 108 neurons 4, 24 and 48 h post-surgery. The vast majority (~90%) of cholinergic MBN neurons exhibited APP immunoreactivity (Fig. 1c, 2a″, Table 1), whereas only a smaller fraction (20–30%) of non-cholinergic MBN neurons was immunoreactive for APP. NMDA infusion resulted in a massive loss of ChAT immunoreactivity that became apparent as early as 4 h post-lesion and persisted throughout the survival period investigated (Fig. 2b–d). As Table 2 shows, a significant reduction of the ChAT-ir neuron population (cell numbers: 1283 $\pm$ 352, 4 h; 885 $\pm$ 104, 24 h; 1236 $\pm$ 266, 48 h) was evident relative to the contralateral MBN. In parallel with the NMDA-induced cholinergic breakdown, the number of NeuN-ir neurons also exhibited a significant decline at each time-point investigated (cell numbers: 2407 $\pm$ 361, 4 h; 2060 $\pm$ 166, 24 h; 2656 $\pm$ 523, 48 h; Fig. 2b′–c′, Table 2). Interestingly, NMDA infusion did not alter the ratio of ChAT-ir and NeuN-ir neurons in the damaged MBN (Table 1). Neuronal APP immunoreactivity displayed a similar temporal profile as the above markers with a significant decrement throughout the post-lesion interval investigated (Table 2). It is worth noting that more than 90% of the cholinergic neurons withstanding NMDA excitotoxicity also retained their APP immunoreactivity (Fig. 2d″; Table 1). On the other hand, the ratio of NeuN-positive/APP-ir nerve cells declined after NMDA infusion, reaching

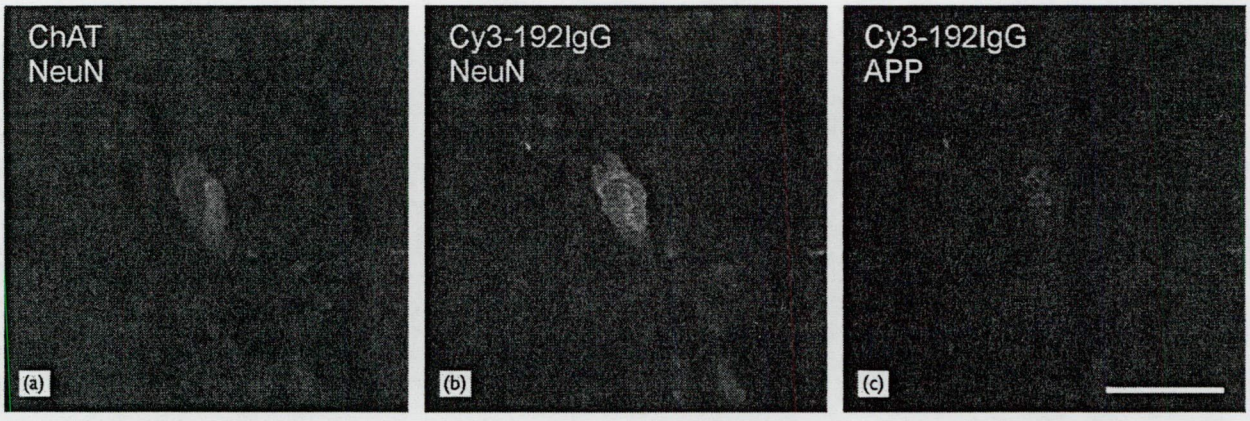

Fig. 1. A series of confocal laser-scanning microscopy images of an *in vivo*-labeled cholinergic neuron immunoreactive for amyloid precursor protein (APP) in rat nucleus basalis under control conditions. Pairs of color-coded images were obtained following quadruple immunolabeling for APP, Cy3-192IgG, neuron-specific nuclear protein (NeuN), and choline-acetyltransferase (ChAT). NeuN, ChAT and APP were revealed with Cy2 (green), AMCA (blue, **a**) and Cy5 (color-coded in purple) respectively, while Cy3-192IgG appears in red (**b**). The concomitant appearance of Cy3-192IgG and APP (color-coded in purple; **c**) denotes constitutive APP expression of cholinergic projection neurons in the nucleus basalis. Bar = 40 μm.

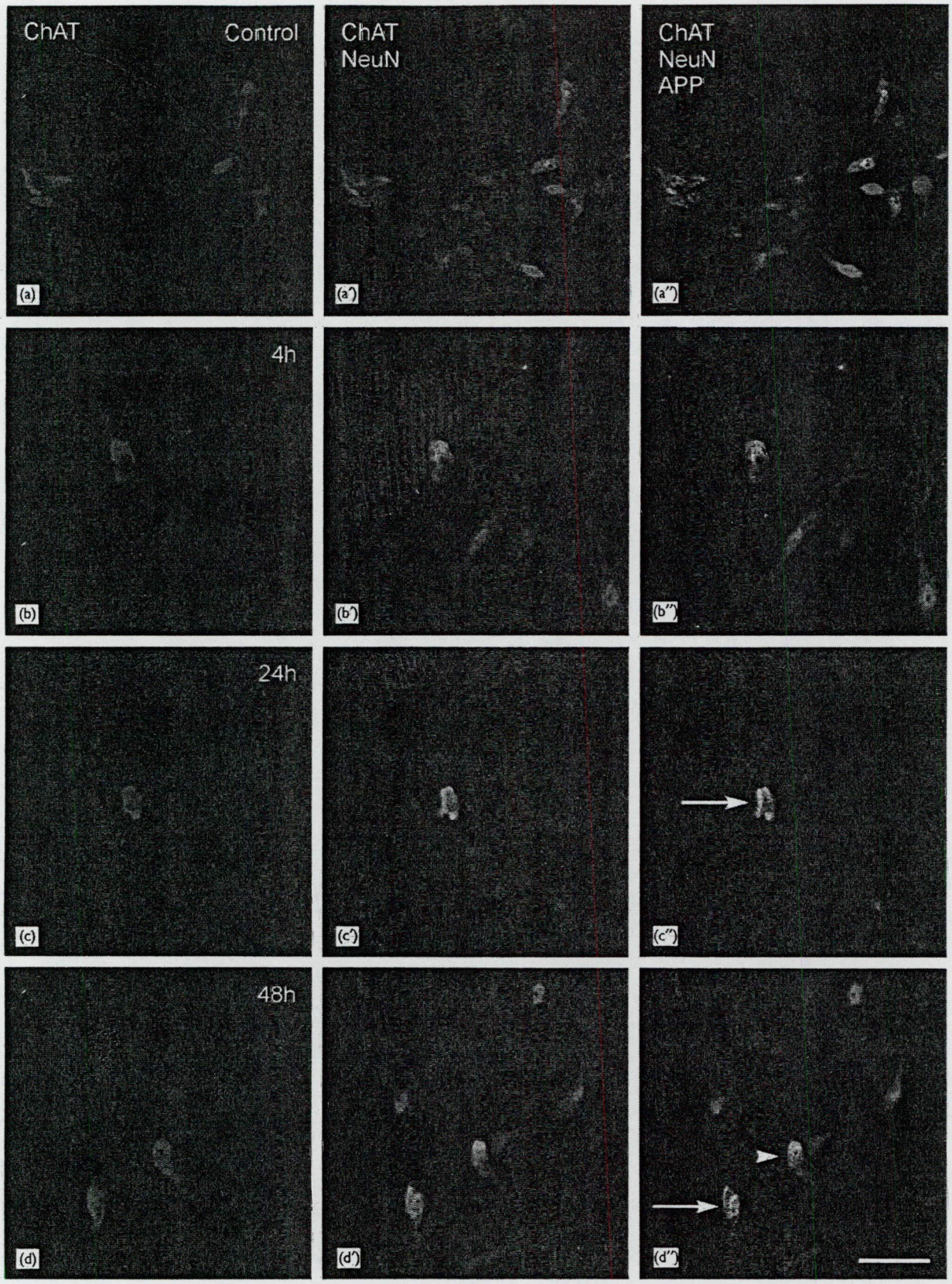
ChAT
Control
ChAT
NeuN
ChAT
NeuN
APP
(a)
(a′)
(a″)
4h
(b)
(b′)
(b″)
24h
(c)
(c′)
(c″)
48h
(d)
(d′)
(d″)

Table 1. Cellular co-localization of neuron-specific nuclear protein (NeuN), choline-acetyltransferase (ChAT) and amyloid precursor protein (APP) immunoreactivities 4, 24, and 48 h after NMDA infusion in the rat magnocellular nucleus basalis (MBN).

Time (h)	Hemisphere	$NeuN^+/ChAT^+$ (%)	$ChAT^+/APP^+$ (%)	$NeuN^+/APP^+$ (%)
4	Sham lesioned	53.7 ± 10.5	90.1 ± 2.2	56.4 ± 4.4
	NMDA lesioned	40.2 ± 15.0	93.6 ± 4.3	49.7 ± 4.2
24	Sham lesioned	46.2 ± 4.9	95.1 ± 1.0	49.6 ± 7.1
	NMDA lesioned	40.7 ± 10.5	90.1 ± 2.8	25.9 ± 11.1
48	Sham lesioned	48.1 ± 7.5	94.5 ± 1.7	79.5 ± 4.7
	NMDA lesioned	45.3 ± 10.8	91.8 ± 2.7	64.6 ± 6.9

NMDA infusion in the MBN did not influence the percentage co-localization of the cellular markers investigated, compared to sham-operated conditions at any of the post-lesion time-points investigated. Co-localization of each pair of the cellular markers was determined using a Zeiss Axioplan fluorescence microscope fitted with appropriate double band pass filters for the concomitant detection of immunosignals. Data are expressed as means ± s.e.m. ($n = 4$/group).

Table 2. Short-term effect of NDMA infusion in the magnocellular nucleus basalis (MBN) on the loss of neuron-specific nuclear protein (NeuN), choline-acetyltransferase (ChAT) and amyloid precursor protein (APP) immunoreactivities.

Time (h)	$ChAT^+$ (% loss of neurons)	$NeuN^+$ (% loss of neurons)	APP^+ (% loss of neurons)
4	42.0 ± 8.4*	47.4 ± 5.7**	52.6 ± 6.4**
24	65.1 ± 3.9**	52.5 ± 7.5*	51.8 ± 16.8*
48	54.4 ± 8.1**	46.9 ± 11.9*	56.8 ± 3.6**

The number of nerve cells immunoreactive for NeuN, ChATor APP was determined in both the sham- and NMDA-lesioned MBN 4, 24 and 48 h post-surgery. The relative value of cell loss for each cellular marker was calculated as the percentage difference between the numbers of immunoreactive neurons at NMDA- and sham-lesioned sides of the brain. The cell counting protocol is referred to in Materials and Methods. Statistically significant differences between the NMDA-lesioned and control MBN at particular post-lesion time-points: $^{**}p < 0.01$, $^{*}p < 0.05$ (paired *t*-test). Data are expressed as means ± s.e.m. ($n = 4$/group).

maximum 24 h post-lesion (25.9 ± 11.1%, Table 1), that points to a marked loss of APP immunoreactivity of non-cholinergic MBN neurons.

It is noteworthy that APP immunoreactivity was observed in neural structures that were immunonegative for both ChAT and NeuN following NMDA infusion in the MBN (Fig. 2b″–d″). The progressive post-lesion appearance of this immunoreactivity suggests a glial origin for such APP labeling [10].

DISCUSSION

Major novel findings of the present study include that all cholinergic MBN neurons are positive for NeuN, while double-immunofluorescence labeling with ChAT and NeuN can also be utilized to visualize non-cholinergic nerve cells in the basal forebrain. Interestingly, the ratio of NeuN and ChAT co-localization was ~50%. The NeuN-labeled non-cholinergic neuron population of the MBN was as sensitive to acute excitotoxicity as the cholinergic neurons when exposed to 60 mM NMDA. The majority of cholinergic neurons express APP both under control and acute excitotoxic conditions. In contrast, a smaller percentage of NeuN-ir non-cholinergic neurons exhibits APP immunoreactivity under physiological circumstances that further decreases shortly after exposure to NMDA.

BF nuclei comprise neurons with a broad neurochemical heterogenity. Whereas the absolute numbers of cholinergic neurons under control conditions detected in our study corroborate previous data [21–23], the amount of NeuN-ir nerve cells seems relatively low based on the assumption that NeuN can be utilized as a general neuronal marker [19]. Previous studies of ours [21] and others [23] point to total cell numbers in the MBN a magnitude higher than those detected by NeuN. Hence, we assume that the BF, similar to e.g. the cerebellum [19], contains neurons that are immunonegative for NeuN. To this end, NeuN staining can be regarded as a useful marker to tag subpopulations of BF neurons. Further studies are yet to be performed to reveal the neurochemical nature of NeuN-ir non-cholinergic, as well as of NeuN-immunonegative nerve cells.

The loss of NeuN-ir non-cholinergic neurons paralleled the decline of cholinergic nerve cells after the NMDA-induced excitotoxic challenge. The similarly reduced numbers of neurons reactive for NeuN or ChAT supports this conclusion (Table 2) concomitant with the preserved ratio of co-localization of the two neuronal markers (Table 1) throughout the post-lesion period investigated. In functional terms, the simultaneous loss of ChAT and NeuN

Fig. 2. Short-term effects of NMDA excitotoxicity on distinct neuron populations in rat magnocellular nucleus basalis (MBN). The triple immunofluorescence labeling for choline-acetyltransferase (ChAT, **a–d**), neuron-specific nuclear protein (NeuN, **a′–d′**), and amyloid precursor protein (APP, **a″–d″**) allowed visualization of distinct subpopulations of MBN neurons. The immunocytochemical markers were captured by confocal laser-scanning microscopy and color-coded as follows: ChAT in red (Cy3), NeuN in green (Cy2) and APP in blue (AMCA). Structures co-expressing the three cellular markers appear white (*arrows*). Whereas a dense network of cholinergic and intermingled non-cholinergic neurons was seen under control conditions (a–a″), excitotoxic damage to both cholinergic and non-cholinergic subpopulations of MBN neurons became evident at 4 h post-lesion (b–b″) and was present throughout the survival periods investigated (c–c″, d–d″). Note the enhanced APP immunoreactivity at the different post-lesion time-points (b″,c″,d″), compared to controls (a″). Arrowhead in d″ points to a cholinergic MBN neuron with low APP immunoreactivity. Bar = 50 μm.

immunoreactivities suggests that at least a subset of non-cholinergic neurons is as sensitive to acute excitotoxicity as cholinergic nerve cells. As neurons expressing different CaBPs were present 4 and 24 h after NMDA infusion in the MBN (Härtig W and Harkany T, unpublished observations), we presume that glutamatergic or peptidergic neurons might form the non-cholinergic neuron population that is sensitive to NMDA excitotoxicity. It remains to be elucidated, however, whether the response of cholinergic and distinct non-cholinergic MBN neurons to NMDA excitotoxicity is similar as a function of increasing NMDA concentration.

It is a widely accepted phenomenon that cholinergic activity directly modulates APP expression in the brain [14–16,22], and *vice versa*, that constitutive APP overexpression leads to the reorganization of cortical cholinergic terminals [24]. It remains elusive, however, whether the increased APP concentration in the cerebral cortex after subcortical cholinergic denervation [14,15] is due to the temporary overt APP expression of degenerating cholinergic and/or non-cholinergic cortical projections, represents a sustained post-synaptic response (e.g. hypersensitivity), or both. Our data on APP immunolabeling demonstrate that cholinergic MBN neurons abundantly express APP both under control, as well as under excitotoxic conditions. Previous studies utilizing longer survival periods [10] demonstrated that severely damaged, and probably apoptotic, MBN neurons exhibit significantly increased APP immunoreactivities, whereas those withstanding the excitotoxic challenge are only moderately labeled. Remarkably, the majority of NeuN-ir non-cholinergic MBN neurons appeared to be APP-immunonegative, and a decrease of their APP immunoreactivity was demonstrated after NMDA infusion. These observations together with the fast anterograde transport of APP in neuronal projections [25] indicate that cholinergic neurons in the BF, abundantly express APP and may play a primary role in regulating the cortical APP load after BF lesions.

CONCLUSIONS

The parallel decline of ChAT and NeuN immunoreactivities after NMDA infusion demonstrates that a subset of non-cholinergic neurons exists in the rat MBN that is sensitive to acute excitotoxic injury to a degree comparable to that of cholinergic nerve cells. From a methodological point of view it is noteworthy that ~4500–5000 neurons were immunoreactive for NeuN in the MBN. As previous findings [21,23] suggest significantly higher numbers of neurons in the MBN, further studies are awaited to determine whether NeuN only labels a subset of BF neurons, or Nissl staining-based quantification protocols overestimated the number of nerve cells in the rat BF. Our neuroanatomical data also indicate that cholinergic neurons can be regarded as one of the major sources of APP in the BF under both control and pathological conditions. In contrast, only a limited portion of NeuN-ir non-cholinergic neurons is APP immunoreactive that further decreases after exposure to NMDA. Taking the rapid increase of cortical APP expression after MBN lesions into account [14,15], it seems likely that excess production of APP by cholinergic BF neurons and subsequent fast axonal transport of APP to the cerebral cortex [25] might be in causal relationship with the cortical changes of APP concentrations.

REFERENCES

1. Mesulam MM, Mufson EJ, Wainer BH *et al. Neuroscience* **10**, 1185–1201 (1983).
2. Semba K. *Behav Brain Res* **115**, 117–141 (2000).
3. Gaykema RP, Luiten PGM, Nyakas C *et al. J Comp Neurol* **293**, 103–124 (1990).
4. Riedel A, Härtig W, Seeger G *et al. J Chem Neuroanat* **23**, 75–104 (2002).
5. Bender R, Plaschke M, Naumann T *et al. J Comp Neurol* **372**, 204–214 (1996).
6. Everitt BJ and Robbins TW. *Annu Rev Psychol* **48**, 649–684 (1997).
7. Kása P, Rakonczay Z and Gulya K. *Prog Neurobiol* **52**, 511–535 (1997).
8. Harkany T, Ábrahám I, Kónya C *et al. Rev Neurosci* **11**, 329–382 (2000).
9. Harkany T, Grosche J, Mulder J *et al. Neuroscience* **108**, 611–627 (2001).
10. Harkany T, Dijkstra IM, Oosterink BJ *et al. Neuroscience* **101**, 101–114 (2000).
11. Wenk GL. *Behav Brain Res* **72**, 17–24 (1995).
12. D'Orlando C, Fellay B, Schwaller B *et al. Brain Res* **909**, 145–158 (2001).
13. Mattson MP, Rychlik B, Chu C *et al. Neuron* **6**, 41–51 (1991).
14. Wallace WC, Bragin V, Robakis NK *et al. Mol Brain Res* **10**, 173–178 (1991).
15. Wallace W, Ahlers ST, Gotlib J *et al. Proc Natl Acad Sci USA* **90**, 8712–8716 (1993).
16. Roßner S, Ueberham U, Schliebs R *et al. Prog Neurobiol* **56**, 541–569 (1998).
17. Härtig W, Seeger J, Naumann T *et al. Brain Res* **808**, 155–165 (1998).
18. Wu M, Shanabrough M, Leranth C *et al. J Neurosci* **20**, 3900–3908 (2000).
19. Mullen RJ, Buck CR and Smith AM. *Development* **116**, 201–211 (1992).
20. Paxinos G and Watson C. *The Rat Brain in Stereotaxic Coordinates*. 2nd edn. Sydney: Academic Press; 1986.
21. Harkany T, Mulder J, Horvath KM *et al. Neuroscience* **108**, 629–642 (2001).
22. Leanza G. *Neurosci Lett* **257**, 53–56 (1998).
23. Smith ML and Booze RM. *Neuroscience* **67**, 679–688 (1995).
24. Wong TP, Debeir T, Duff K *et al. J Neurosci* **19**, 2706–2716 (1999).
25. Koo EH, Sisodia SS, Archer DR *et al. Proc Natl Acad Sci USA* **87**, 1561–1565 (1990).

Acknowledgements: This work was supported by grants from the Hungarian National Science Foundation (OTKA, F035254 to T.H., T034895 to B.P.), the Deutsche Forschungsgemeinschaft (DFG, No. Ha 2211/2-1 to W.H.), and the Interdisciplinary Center for Clinical Research at the University of Leipzig (IZKF 01 KS 9504 to J.G.).